Journal of Sound and Vibration (2002) **254**(4), 635–676
doi:10.1006/jsvi.2001.4112, available online at http://www.idealibrary.com on IDEAL®

A FAST TIME–DOMAIN INTEGRATION METHOD FOR COMPUTING NON-STATIONARY RESPONSE HISTORIES OF LINEAR OSCILLATORS WITH DISCRETE-TIME RANDOM FORCING

J. F. DUNNE

School of Engineering and Information Technology, The University of Sussex, Falmer, Brighton, BN1 9QT, England

(*Received* 5 *December* 2000, *and in final form* 3 *August* 2001)

A new approach is presented for computing displacement histories of single linear oscillators with arbitrarily light damping and general forcing—of particular use for efficient Monte Carlo simulation of modal systems with ultra-light damping and very broadband non-Gaussian excitation. Solution methods are initially presented within a state transition context, to show limitations of FFT solutions, and to establish, for long-run non-stationary stochastic analysis via fast Laplace, the need for appropriate zero-padding, high cut-off frequency, and fixed-step sampling. Truncation errors arising in single-transition time-domain convolution are then examined via the Euler–Maclaurin summation formula. Errors are shown to be minimum when transition intervals are chosen as integer multiples of the damped natural period, precisely where the $O(\Delta\tau^2\Delta f')$ error can be evaluated, and the velocity transition equation can be dispensed with. The paper shows that an optimum $O(\Delta\tau^4\Delta f''')$ integration scheme can be used for fast time-domain convolution in a two-stage algorithm. First, phased-pairs of accurate displacements are efficiently predicted at selected transition times. These are then used as boundary conditions in adaptive Chebychev polynomial solution giving continuous displacement histories for selected cycles—this considerably reduces the number of multiplications and integrations normally required. Two-stage integration turns out to be at least 100 times faster than explicit short-transition time-domain solution, and for general applications, at least as fast as the Laplace/IFFT approach. But for non-stationary probability density estimation, involving far-future history prediction the speed advantage over fast Laplace can be enormous.

1. INTRODUCTION

Small-amplitude motion of lightly damped space structures with broadband random loading, can be modelled to moderately high frequency with constant-coefficient linear differential equations [1, 2]. Very light damping, however, can cause serious vibration problems in space structures, where much effort has gone into finding additional damping through better understanding of materials [3, 4], or through active control [5]. Intrinsic damping levels in small space structures can be as low as 0·2% critical for low-frequency modes, but very much less than 0·1% for the higher modes of larger structures. Random forcing can occur on space structures as continuous or intermittent broadband noise (perhaps with screech tones) through turbulent flow in ducting and pipes [6], from jet or thruster noise [7], from flow inside high-speed machinery [8, 9] and from the use of

0022-460X/02/$35.00

pyrotechnic devices [10]. Typically, this is characterized by a very high-frequency range, departure from normal or well-known distributions, and possible quiet periods, through intermittent activity on-board. With these characteristics, non-stationary stochastic analysis offers a key route to "worst-case" response prediction. Indeed, for the very worst case, zero structural damping should be used since this most likely gives largest response. But the time-scales for such non-stationary analysis can be relatively long, making much of the response build-up of little importance, deeming "far-future" statistics of interest. Accurate and efficient "far-future" prediction of structural vibration using dynamic models with ultra-low damping, can be difficult for both deterministic and stochastic analysis.

Non-stationary stochastic analysis of m.d.o.f. linear systems can be approached by using (1) analytical methods, or (2) via Monte Carlo simulation (where pseudo-deterministic response histories are generated numerically and then used in statistical analysis). The accuracy of analytical methods depends initially on having an adequate statistical description of the excitation. This requires sufficient field data to fit an input model (via techniques similar to those used for seismic data [11, 12]). Probabilistic models however are "information intensive" [13], and in some cases input data requirements may be difficult to meet. Monte Carlo methods by contrast, can be applied to any number of input histories, but to estimate output statistics, enough samples are required. Indeed if design probabilities are low, a very large ensemble is needed. In assessing the best approach, i.e., analytical versus Monte Carlo methods, this depends both on meeting sample size requirements and accuracy.

Efficient analytical methods have been developed for non-stationary response analysis of m.d.o.f. linear systems [14–17] by assuming a modulated power spectrum fully describes the input process. These methods give output correlation matrices or power spectra under general input conditions. Exact probabilities can also be obtained, but for normal excitation only. Efficient methods have also been developed to approximate non-stationary crossing or extreme value statistics for s.d.o.f. systems with normal forcing [18–20]. The FPK equation [21] also offers a route to transition probabilities for low dimension systems with normal or functionally related forcing, but the form of numerical solution usually required is often very demanding. Non-normal excitation can cause significant prediction errors if normality is otherwise assumed [22, 23], and several methods have been developed to handle systems driven by certain types of non-normal excitation. Two methods are of significance, namely use of the space moments method [24] for systems driven by a filtered train of pulses randomly distributed in time, and the maximum entropy method [25] for polynomial functions of normal forcing. A moment differential approach has also been developed for polynomial functions of delta-correlated excitation [26] which, for external and parametric excitation, satisfies an important closure property [27, 28]. C-type Gram Charlier series have also been applied (to a beam structure) with delta-correlated excitation [29]. Wholly analytical methods are computationally efficient, but can only be applied when the excitation assumptions are valid [30]. None of the methods cited give exact response probabilities for general types of random excitation. Monte Carlo methods can do this, but often at great computational cost.

Monte Carlo simulation does indeed offer a practical alternative for ultra-light damped systems using measured or simulated excitation of high-bandwidth [31], provided predictions of individual response histories remain accurate. Displacement prediction over a long duration requires accuracy in amplitude and phase be maintained, as for steady state response, but in non-stationary analysis, there is a greater computational burden because a higher cut-off frequency is needed. Fast displacement prediction for damped linear systems, can be obtained using superposition and standard discrete FFT techniques [32]. Greater efficiency can be obtained for normal mode systems, by reduction to uncoupled

second order equations. When damping becomes light, constant-coefficient linear models tend, in the limit, to normal mode systems. As damping approaches zero, however, computational demand using FFT explodes, justifying alternatives such as Laplace transform [33], or use of time-domain methods via direct Duhamel integration [34–36] or step-by-step schemes [37]. Numerous simple integration schemes have been developed for arbitrary damping levels and general forcing in continuous-time (a good example of a simple recursive scheme is given in reference [38]). These algorithms tend to be computationally very slow. Recently, a fast continuous-time method has been developed by exploiting special (non-linear) interpolation functions for use with discrete excitation [39], although when used with random histories, error analysis is difficult. Indeed, it has been clearly recognized [40], that no step-by-step algorithm can ever be exact for use with discrete-time random excitation.

In choosing a numerical method for use in Monte Carlo simulation of systems with ultra-light damping and ultra-high-bandwidth discrete random excitation, a Laplace transform solution, using single-section DFFT, will usually be faster than any time-domain approach. However, a long simulation involving one single section, may require massive memory, such that much of the speed advantage over a time-domain solution is lost. Moreover, there is scope for speeding-up time-domain methods by focusing on far-future response prediction and exploiting quiet periods. A discrete-time method is also much more preferable for simulating the required target statistical properties of the excitation because unlimited length sections can be constructed much faster than parametrically generated histories, and also because measured histories are often only available in discrete form [40]. Three resulting discrete-time integration issues must, however, be addressed before any benefit of speeding-up can be fully realized. The first problem with discrete random histories arises because sampling-rate and step size are intrinsically linked. Local step-size control is therefore not possible, since this would cause a local change in excitation intensity, ruling-out the use of Gaussian quadrature in Duhamel integration, or variable time-step ODE solvers [37]. The second problem arises because it is impossible to obtain exact derivatives of a discrete random process, and therefore the accuracy of higher order integration methods always remains uncertain. And third, since non-stationary prediction with very broadband excitation, often requires extremely high sampling rate, the cut-off frequency must be considered more carefully than for stationary simulation. The stationary approach used in reference [41] for example, is not appropriate, but neither are sophisticated infinite-bandwidth algorithms [42] needed, since the excitation will ultimately always be band-limited. These difficulties justify the creation of a well-understood time-domain method for computing non-stationary histories of single modal equations with discrete random excitation. This would be useful for displacement prediction if it could (1) maintain accuracy in amplitude and phase over long durations, (2) exploit excitation quiet periods, and (3) could very efficiently focus on "far-future" sections of a simulation.

In this paper, a new time-domain approach is developed for computing displacement histories of single linear oscillators with arbitrarily light damping and ultra-high-bandwidth discrete forcing. The main objective is to create a fast method to meet the three requirements (1–3) whilst retaining full excitation bandwidth. Initially, several response methods are examined, and the importance of cut-off frequency demonstrated. The Euler–Maclaurin summation formula is then used for truncation error analysis arising within a convolution integration approach to obtain individual response transitions. This is used to establish the apparent "worst", and "best", choice of transition length. Errors arising at both the "worst" transition length (namely the integration step size $\Delta\tau$), and at the "best" (an integer multiple of the damped natural period) are examined in detail within sections 4 and 5, culminating in

the creation of an optimum integration scheme. Multi-transition error propagation for these two cases is examined in section 6. In section 7, an adaptive Chebychev polynomial boundary-value solution for constructing detailed histories is developed for use with the optimum integration scheme. A fast algorithm is given in section 8 and compared with two independent solution methods to establish its efficiency for oscillator response history prediction involving intermittent discrete random forcing with quiet periods, and for "far-future" response prediction. The method is then demonstrated in a Monte Carlo approach to non-stationary density estimation with general forcing.

2. RESPONSE HISTORY COMPUTATION: VERY LIGHTLY DAMPED OSCILLATORS

In developing a fast time-domain method, attention is focused on an m.d.o.f. normal mode model

$$[\mathrm{M}]\ddot{\underline{Z}} + [\mathrm{C}]\dot{\underline{Z}} + [\mathrm{K}]\underline{Z} = \underline{p}(t) \tag{1}$$

which is often used to study small displacement-forced vibration via uncoupled oscillator equations

$$\ddot{q}_k + 2\xi_k\omega_{nk}\dot{q}_k + \omega_{nk}^2 q_k = Q_k(t), \tag{2}$$

which are usually obtained with a normal co-ordinate transformation $\underline{Z} = [\mathbf{X}]q(\underline{t})$. If the modal damping factors ξ_k of the N-d.o.f. system are assumed in a preliminary design to be virtually zero, the question then for the case $\xi_k \to 0$ is how the forced modal equations can be solved efficiently in the time-domain, when the modal excitation functions are either continuous or intermittent broadband random noise up to 20 kHz, where, in particular, only the final stages of a long simulation are of interest. Before developing a new time-domain solution approach to this problem in sections 3 and 5, via an explicit numerical Duhamel approach, state transition equations are presented, and the problem with convolution via FFT is highlighted as $\xi_k \to 0$. Then a Laplace transform/IFFT approach is developed and used to show the importance of bandwidth cut-off frequency for transient responses. (A list of symbol definitions is given in Appendix A.)

2.1. LINEAR STATE TRANSITION EQUATIONS FOR SECOND ORDER OSCILLATORS

The initial-value problem associated with modal equation (2), can be put in state-space form,

$$\dot{\underline{x}} = A\underline{x} + B\underline{u}, \tag{3}$$

where (appropriately dropping suffix k) the solution from initial time t_0 to any time t, is given as

$$\underline{x}(t) = \mathrm{e}^{(t-t_0)A}\underline{x}(t_0) + \int_{t_0}^{t} \mathrm{e}^{(t-\tau)A} B(\tau)\,\underline{u}(\tau)\,\mathrm{d}\tau, \tag{4}$$

where $\underline{x}^{T}(t) = [q(t)\ \dot{q}(t)]$ is a two-state vector. For finite transitions, displacement and velocity are

$$q(t) = \phi_1(t - t_0)q(t_0) + \phi_2(t - t_0)\dot{q}(t_0) + \int_{t_0}^{t} \phi_2(t - \tau)\,Q(\tau)\,\mathrm{d}\tau \tag{5}$$

and

$$\dot{q}(t) = \phi_3(t - t_0)q(t_0) + \phi_4(t - t_0)\dot{q}(t_0) + \int_{t_0}^{t} \phi_4(t - \tau)\,Q(\tau)\,\mathrm{d}\tau, \tag{6}$$

where the individual state transition functions are defined as

$$\phi_1(t) = \frac{(-\rho_2 \mathrm{e}^{\rho_1 t} + \rho_1 \mathrm{e}^{\rho_2 t})}{(\rho_1 - \rho_2)}, \tag{7}$$

$$\phi_2(t) = \frac{\mathrm{e}^{\rho_1 t} - \mathrm{e}^{\rho_2 t}}{(\rho_1 - \rho_2)} = h(t) = \frac{\mathrm{e}^{-\xi\omega_{nk}t}}{\omega_{dk}} \sin(\omega_{dk}t) \quad \text{for } \xi < 1, \tag{8}$$

$$\phi_3(t) = \frac{(-\rho_1\rho_2 \mathrm{e}^{\rho_1 t} + \rho_1\rho_2 \mathrm{e}^{\rho_2 t})}{(\rho_1 - \rho_2)} = \dot{\phi}_1(t), \tag{9}$$

$$\phi_4(t) = \frac{\rho_1 \mathrm{e}^{\rho_1 t} - \rho_2 \mathrm{e}^{\rho_2 t}}{(\rho_1 - \rho_2)} = \dot{\phi}_2(t) = \dot{h}(t). \tag{10}$$

The function $h(t)$, appearing in equations (8) and (10), is the impulse response function, and ρ_1 and ρ_2 are complex conjugate roots of the characteristic equation, namely

$$\rho_1 = -\xi_k\omega_{nk} + \mathrm{j}\omega_{nk}\sqrt{1 - \xi_k^2}, \tag{11}$$

$$\rho_2 = -\xi_k\omega_{nk} - \mathrm{j}\omega_{nk}\sqrt{1 - \xi_k^2}. \tag{12}$$

The convolution integrals in equations (5) and (6) can be obtained explicitly in many different ways—here both the discrete Fourier transform and the discrete Laplace transform approaches are examined.

2.2. CONVOLUTION VIA FOURIER TRANSFORM USING FFT

Displacement prediction over a single transition using equation (5), can be obtained via superposition using the complex frequency response function $\mathrm{H}(\mathrm{j}\omega)$ associated with equation (2), and the excitation Fourier transform $Z_{Q_k}(\mathrm{j}\omega)$. The complex response $Z_{q_k}(\mathrm{j}\omega)$ is then given by

$$Z_{q_k}(\mathrm{j}\omega) = \mathrm{H}(\mathrm{j}\omega)Z_{Q_k}(\mathrm{j}\omega) \tag{13}$$

from which the time response $q_k(t)$ can be obtained by inverse Fourier transform. For non-zero damping, radix 2 FFT/IFFT algorithms allow fast completion of these processes at discrete times $t_i = i\Delta$ where $i = 1, \ldots, n$, gives discrete frequencies $f_i = i/(2\Delta n)$ Hz. Although processing via FFT + IFFT, only requires $(n/2)\ (2\log_2(n) + 1)$ floating point operations, to avoid the problem of *overlap*, two durations need to be considered, namely the initial section duration T_{max}, and a zero-padding duration T_{pad}. Since T_{pad} tends to infinity as $\xi_k \to 0$, a large number n is needed for very light damping. The combination of

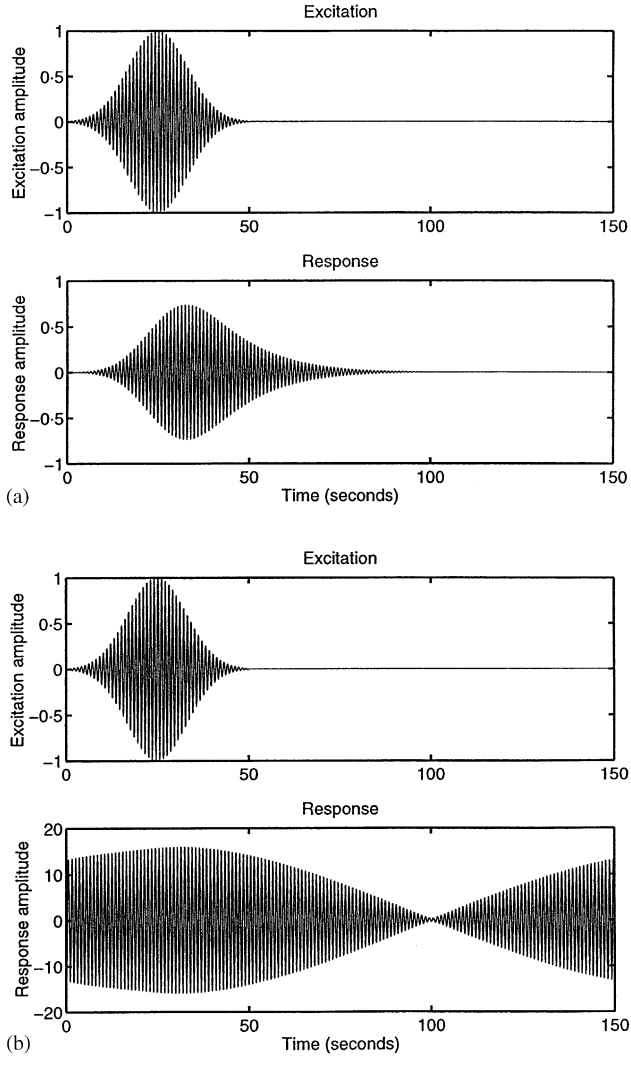

Figure 1. Oscillator excitation and displacement response to modulated sinewave input obtained via frequency-domain convolution using FFT: (a) $\xi = 0{\cdot}01$ (1%); (b) $\xi = 0{\cdot}0001$ (0·01%).

very broadband excitation and very light damping means that an extremely large number of discrete samples is needed to maintain accuracy. For example, a system requiring $f_{max} = 20$ kHz, and $T_{max} = 200$ s, which also requires $T_{pad} = 10T_{max}$, will need $n = 10^8$ discrete points—this can create major storage and computational problems. Figure 1(a) shows the predicted displacement of a transiently forced system obtained by FFT for $\xi_k = 0{\cdot}01$ (1%) with appropriate choices of T_{max} and T_{pad}. Figure 1(b) shows the corresponding prediction for $\xi_k = 0{\cdot}0001$ (0·01%) using the same value of T_{pad}—the predicted displacement is in error by a factor of 10 and requires more than 100-fold increase in computation to obtain an accurate displacement response. This shows-up a limitation with the FFT approach. Another is that FFT cannot exploit excitation quiet periods, since the same computational demand is required, even though at certain times there may be zero input in the time domain. A time-domain solution better suited to take advantage of quiet periods is addressed in sections 3 and 5.

2.3. DIRECT SOLUTION VIA LAPLACE TRANSFORM AND IFFT

The solution to equation (2) can also be obtained directly via Laplace transform using a complex Fourier series representation of the excitation Q in equation (2) in the form

$$\ddot{q}_k + 2\xi_k\omega_{nk}\dot{q}_k + \omega_{nk}^2 q_k = \sum_{m=-\infty}^{\infty} C_m \, e^{j\omega_m(t-t_0)}. \tag{14}$$

By setting, for convenience, the initial conditions to zero, the Laplace transform of equation (14) expanded into partial fractions, gives an s-domain equation

$$\bar{q}_k(s) = \sum_{m=-\infty}^{\infty} \left[\frac{\alpha_{1m}}{s-\rho_1} + \frac{\alpha_{2m}}{s-\rho_2} + \frac{\alpha_{3m}}{s-j\omega_m} \right], \tag{15}$$

which on transforming back to the time-domain (and with reintroduction of t_0) gives the solution

$$\begin{aligned} q_k(t) &= \sum_{m=-\infty}^{\infty} [\alpha_{1m} e^{\rho_1(t-t_0)} + \alpha_{2m} e^{\rho_2(t-t_0)} + \alpha_{3m} e^{j\omega_m(t-t_0)}] \\ &= e^{\rho_1(t-t_0)} \sum_{m=-\infty}^{\infty} \alpha_{1m} + e^{\rho_2(t-t_0)} \sum_{m=-\infty}^{\infty} \alpha_{2m} + \sum_{m=-\infty}^{\infty} \alpha_{3m} e^{j\omega_m(t-t_0)}, \end{aligned} \tag{16}$$

where the coefficients are

$$\alpha_{1m} = \frac{C_m}{(\rho_1 - \rho_2)(\rho_1 - j\omega_m)}, \tag{17}$$

$$\alpha_{2m} = \frac{C_m}{(\rho_2 - \rho_1)(\rho_2 - j\omega_m)}, \tag{18}$$

$$\alpha_{3m} = \frac{C_m}{(j\omega_m - \rho_1)(j\omega_m - \rho_2)}, \tag{19}$$

and where ρ_1 and ρ_2 are the same complex roots given by equations (11) and (12). When $\xi_k = 0$, the solution given by equation (16) holds provided that $\omega_m \neq \omega_{nk}$. When $\omega_m = \omega_{nk}$ for $\xi_k = 0$, the corresponding harmonic term within the summation in equation (16) should be replaced by the term

$$q_{nk}(t) = \frac{jC_{nk}}{2\omega_{nk}^2} [\sin(\omega_{nk}(t-t_0)) - (\omega_{nk}(t-t_0)) \, e^{j\omega_{nk}(t-t_0)}]. \tag{20}$$

Although the last summation in equation (16) can be computed by using an IFFT, the entire equation in this "fast" Laplace solution is in general much slower computationally than the conventional discrete FFT approach of section 2.2 except when damping tends to zero.

For computations involving long durations, both FFT and discrete Laplace solution can be broken down into subsections by using multiple transitions where the solution is obtained via successive transitions using equations (5) and (6). Multiple transitions involve propagation of both displacement and velocity—it will be shown in section 3 that the use of numerical integration for computation of velocity in single transitions can be very

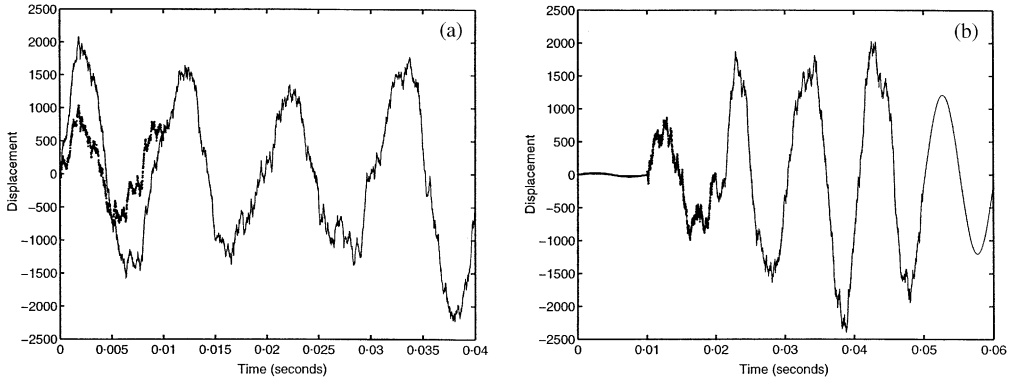

Figure 2. Displacement prediction: zero-padding requirements in Laplace/IFFT method. Single cycle compared with multiple cycle prediction for differentiated (band-limited) white-noise excitation: (a) without zero padding; (b) with zero padding before and after predicted single cycle.

inaccurate when used with discrete random excitation. But it should also be noted that the use of subsectioning in the direct FFT approach or the Laplace/IFFT solution requires appropriate zero padding at the front and rear of each subsection [37]. Figure 2(a) for example, shows the effect of not using zero padding for an oscillator with 0·1% critical damping starting from zero initial conditions driven by (frequency domain) differentiated discrete white noise (the use of which is justified in section 2.4). Figure 2(a) shows four cycles of prediction when using the Laplace/IFFT method, plus just one cycle obtained when using a subsection of the same excitation. Clearly, there is a huge discrepancy between the prediction of the first cycle. Figure 2(b) shows a corresponding prediction when both the four-cycle section of the excitation, and the one-cycle subsection, are both zero-padded by one cycle at the front and rear.

2.4. BANDWIDTH REQUIREMENTS FOR PREDICTION OF NON-STATIONARY HISTORIES

For stationary oscillator response prediction, the bandwidth cut-off for light damping normally need only be chosen at several times the resonant frequency. A potentially important aliasing issue concerns the corresponding cut-off frequency for transient responses, since this has important implications for discretization in general, and for numerical integration in particular. This is demonstrated for an oscillator with 100 Hz natural frequency and 0·1% damping, driven by white noise where the response is obtained via a partial summation in equation (16). Figure 3(a) shows one cycle of the partial summation as an increasing number of harmonics are included, compared with the solution obtained using a bandwidth of 51 kHz. This shows that convergence is rather slow, requiring around 100 harmonics. The Laplace/IFFT solution can also be used to demonstrate this aliasing—two cases are now considered. The effect of excitation filtering is examined for the same oscillator driven by (1) white noise, and (2) derivative noise. Derivative noise is generated here and elsewhere, by processing discrete white noise in the frequency domain via FFT, and is used merely to emulate the effect of using a low cut-off frequency for non-white excitation such as in prematurely truncating a jet noise spectrum [7]. Figure 3(b) shows for discrete white noise excitation, a section of the transient response of the oscillator, driven by discrete white noise both with- and without filtering. In the case

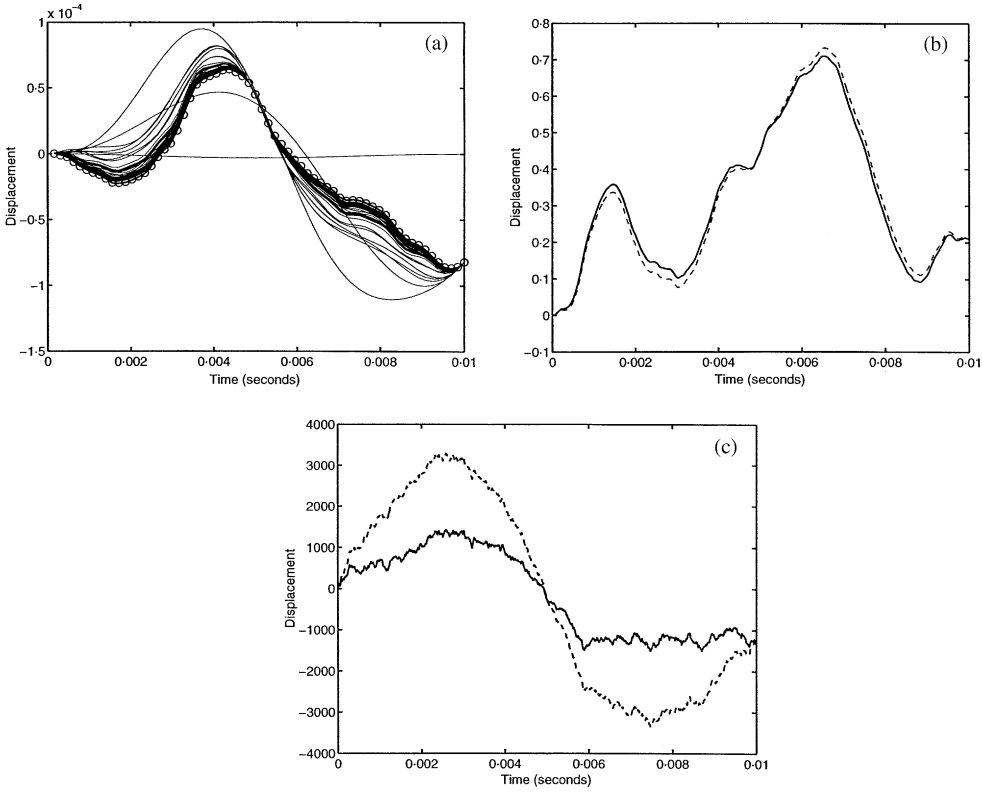

Figure 3. Bandwidth requirements for transient response prediction: (a) partial harmonic sums in Laplace solution for white noise excitation. —, response to unfiltered- and – – –, response to low-pass filtered random excitation; (b) white noise (20% passband); (c) differentiated noise (95% passband).

without filtering, the bandwidth is chosen at 51 kHz, and for the filtered input, frequency domain filtering removes 80% of the excitation frequency content, reducing the cut-off frequency to 10·2 kHz. Figure 3(b) shows that in this example changes in the cut-off frequency of more than 100 times the natural frequency, produce a difference in the transient response. Figure 3(c) shows the same comparison for (non-white) discrete derivative noise (obtained via frequency domain processing) in which only 5% filtering is used to reduce the bandwidth cut-off from 51 to 48·45 kHz. Figure 4(a) shows a sample of the excitation, and Figures 4(b) and 4(c), respectively, show the Fourier sine and cosine coefficients of the unfiltered and filtered section. Figure 3(c) clearly shows that for an extreme case like derivative noise, even a very small change in cut-off frequency, around 500 times the natural frequency, will produce a totally different transient response. In order to clearly and accurately simulate transient responses of a linear oscillator with general types of discrete non-white excitation, the cut-off frequency needs to be selected much greater than the resonant frequency. Indeed, it would appear that the cut-off frequency should be chosen at least up to the frequency where excitation energy has effectively dropped to zero. For transient response prediction, for example, involving jet noise [7] with screech tones, safe discretization will involve very high frequency which can be a problem for time-domain integration unless truncation errors are reduced. These are now examined in detail for single-state transitions via the Euler–Maclaurin summation formula.

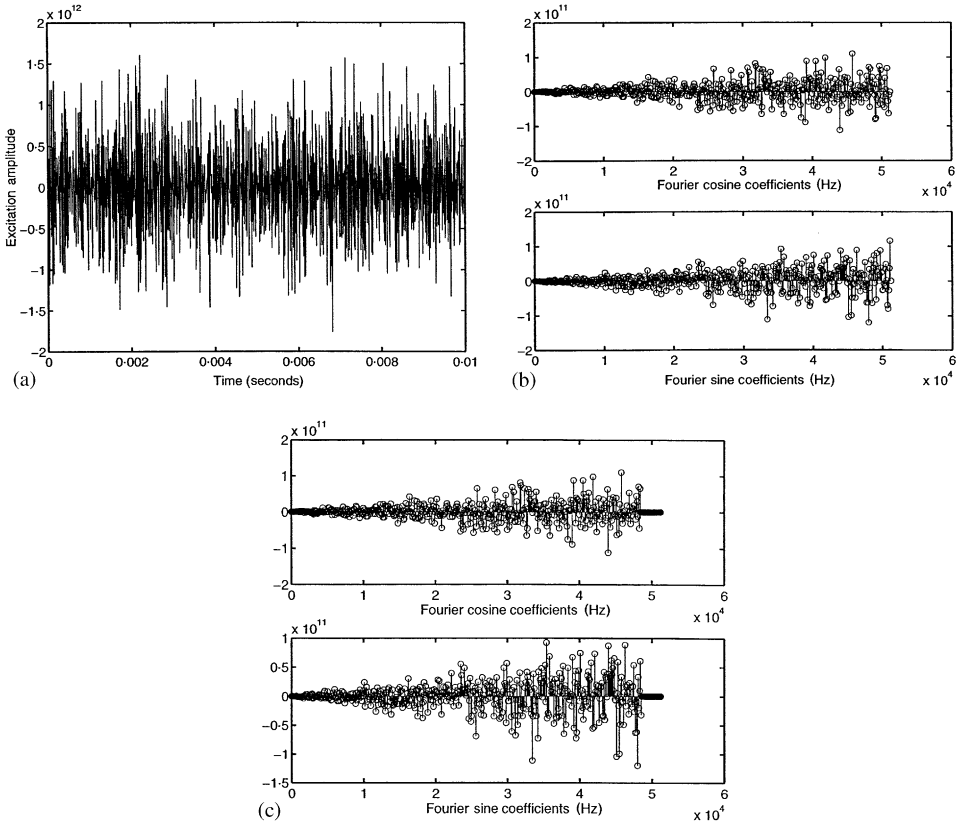

Figure 4. Differentiated noise samples: (a) section of excitation; (b) Fourier series components; (c) unfiltered excitation; partially filtered excitation.

3. TRUNCATION ERROR DEPENDENCE ON TRANSITION INTERVAL CHOICE

To obtain modal displacement and velocity components in the time domain via state transition equations (5) and (6), the following convolution integrals must be obtained explicitly:

$$\mathrm{I}_1 = \int_{t_0}^{t} h(t-\tau)\, Q(\tau)\, \mathrm{d}\tau = \int_{t_0}^{t} G_1(t,\tau)\, \mathrm{d}\tau, \tag{21}$$

$$\mathrm{I}_2 = \int_{t_0}^{t} \dot{h}(t-\tau)\, Q(\tau)\, \mathrm{d}\tau = \int_{t_0}^{t} G_2(t,\tau)\, \mathrm{d}\tau. \tag{22}$$

Numerical convolutions (21) and (22) can be evaluated in the time-domain, by using one of the many numerical integration schemes [37]—this is usually an extremely slow process. Furthermore, only fixed time-step schemes should be used at a high sampling rate, if the aliasing problems described in section 2.4 are to be totally avoided—this leads to a very slow integration with potentially serious truncation error problems for the velocity equation (6). But when only displacement predictions are needed, at a small number of discrete times, then direct convolution can in fact turn out to be much faster than discrete Laplace methods. It is the construction of the detailed solution at very small time steps that

proves to be the computationally expensive part. Now, in using fixed step numerical integration schemes in transition equations (5) and (6), there are actually four ways in which truncation errors can arise. These are the local or global truncation errors associated with (1) a single transition of length $\Delta\tau$ involving a single-step integration of step length $\Delta\tau$, (2) a single transition of length $n\Delta\tau$ involving a multi-step integration of step length $\Delta\tau$, (3) multi-transitions involving a single-step integration of step length $\Delta\tau$, (4) multi-transitions involving multi-step integrations of step length $\Delta\tau$.

In this section, the first step is made by identifying an accurate and efficient numerical integration method with a small truncation error, for use with discrete random forcing. This is done by initially examining for case (2) how truncation errors depend on the choice of transition interval. First, the Euler–Maclaurin summation formula (a generalization of the conventional trapezoidal integration rule) is stated, and higher order error terms identified. Truncation errors in single transitions are then examined, beginning with the derivation of an explicit r.m.s. approximation for use with discrete random excitation—i.e., the usual form of numerical Duhamel integration. This is used to establish whether there is a preferred transition interval.

Now, in selecting a particular integration scheme, since the magnitude of discrete samples of white noise for example, is linked to the step size $\Delta\tau$, as $\Delta\tau \to 0$, the excitation process becomes increasingly irregular with a higher amplitude, such that conventional Taylor series approximations converge slower than normal, if at all. The Euler–Maclaurin summation formula (EMSF) allows this covergence behaviour to be examined in detail for discrete random excitation. Moreover, it forms the way in which most Taylor-series-based higher order methods are generated [37], but it is also noted that higher order does not necessarily translate into higher accuracy. The EMSF proves very appropriate here for examining truncation errors with discrete random noise excitation to enable the most efficient scheme to be identified. This rule is used to obtain the definite integral of some function f, expressed in the form [37]

$$\mathrm{I} = (\Delta\tau)\left[\frac{1}{2}f_1 + f_2 + \cdots + f_{N-1} + \frac{1}{2}f_N\right] - \frac{B_2(\Delta\tau)^2}{2!}[f'_N - f'_1] - \cdots - \frac{B_{2k}(\Delta\tau)^{2k}}{(2k)!}(f_N^{(2k-1)} - f_1^{(2k-1)}) - + \cdots, \tag{23}$$

where the fixed steps are of length $\Delta\tau$, and the truncation error is defined in terms of a (generally divergent) asymptotic expansion, where the coefficients in the series are Bernoulli numbers B_{2k} defined by the generating function

$$\frac{t}{\mathrm{e}^t - 1} = \sum_{n=0}^{\infty} \frac{B_n t^n}{n!}. \tag{24}$$

Apart from $B_1 = -\frac{1}{2}$, the odd coefficients are zero, and the first seven even coefficients from equation (24) are $B_0 = 1$, $B_2 = \frac{1}{6}$, $B_4 = -\frac{1}{30}$, $B_6 = \frac{1}{42}$, $B_8 = -\frac{1}{30}$, $B_{10} = \frac{5}{66}$, $B_{12} = -\frac{691}{2730}$, where, after the first five coefficients, the numerator starts to grow much more rapidly than the denominator causing divergence. When the standard trapezoidal rule is used (i.e., the first summation in equation (23)) the truncation error for an entire interval $t - t_0$ is

$$e = -\frac{(\Delta\tau)^2}{12}[f'(t) - f'(t_0)] + \frac{(\Delta\tau)^4}{720}[f'''(t) - f'''(t_0)] + \cdots \tag{25}$$

and from the bounding properties of an asymptotic expansion, the magnitude of the error for the series truncated after a certain number of terms is always less than twice the magnitude of the first term omitted. This property enables the truncation error for an oscillator with discrete random forcing to be examined, when integrating transition equations (5) and (6).

3.1. RELATIVE TRUNCATION ERROR ESTIMATION FOR SINGLE TRANSITIONS

To examine explicitly the magnitude of the truncation errors when using the first summation in equation (23) (i.e., the standard trapezoidal rule) applied to discrete random excitation, use is made of the ratio

$$r_e = \frac{e_{r.m.s.}}{\mathrm{I}_{r.m.s.}} = \frac{r.m.s.\ \text{error in}\ [t_0, t]}{r.m.s.\ \text{magnitude of integral from}\ [t_0, t]}. \tag{26}$$

This ratio is used to establish statistically the relative importance of including higher terms in equation (23) when the oscillator is driven by band-limited white noise. A theoretical estimate of the first term error ratio for displacement will now be derived, and compared with numerical simulations of the ratio (26) involving first and second term errors for both displacement and velocity. This will require time derivatives of the kernel functions G_1 and G_2 in equations (21) and (22). To avoid confusion, these are shown for the displacement equation (21) by writing

$$f(\tau) = G_1(t, \tau) = h(t, \tau)\, Q(\tau). \tag{27}$$

By treating t as a constant and noting that $\partial h(t-\tau)/\partial\tau = -\dot{h}(t-\tau)$, the required derivatives are

$$f'(\tau) = h(t-\tau)\dot{Q}(\tau) - \dot{h}(t-\tau)\, Q(\tau), \tag{28}$$

$$f''(\tau) = \ddot{h}(t-\tau)Q(\tau) - 2\dot{h}(t-\tau)\,\dot{Q}(\tau) + h(t-\tau)\,\ddot{Q}(\tau), \tag{29}$$

$$f'''(\tau) = \dddot{h}(t-\tau)Q(\tau) + 3\ddot{h}(t-\tau)\,\dot{Q}(\tau) - 3\dot{h}(t-\tau)\,\ddot{Q}(\tau) + h(t-\tau)\,\dddot{Q}(\tau) \tag{30}$$

and a similar set of derivatives for the velocity equation (22), which can be obtained from the set (27)–(30) by replacing $h(t-\tau)$ by $\dot{h}(t-\tau)$, $\dot{h}(t-\tau)$ by $\ddot{h}(t-\tau)$, etc. The theoretical approximation for the first term displacement ratio can be obtained by using $h(t)$ (equation (8)) for $\xi_k \to 0$. For this case, the first error term in equation (25) is

$$e_1 = -\frac{(\Delta\tau)^2}{12}[\sin(\omega_d t)[\dot{Q}(t)\cos(\omega_d t) - Q(t)\omega_d \sin(\omega_d t) - \dot{Q}(t_0)\cos(\omega_d t_0) + Q(t_0)\omega_d \sin(\omega_d t_0)]$$

$$- \cos\omega_d t[\dot{Q}(t)\sin(\omega_d t) + Q(t)\omega_d \cos(\omega_d t)] - \dot{Q}(t_0)\sin(\omega_d t_0) - Q(t_0)\omega_d \cos(\omega_d t_0)] \tag{31}$$

which simplifies to

$$e_1 = -\frac{(\Delta\tau)^2}{12\omega_d}[\dot{Q}(t_0)\sin(\omega_d(t_0 - t)) + Q(t_0)\omega_d \cos\omega_d(t - t_0) - \omega_d Q(t)]. \tag{32}$$

Specializing equation (23) for use with white noise excitation, it is necessary to establish equivalent derivative properties of band-limited discrete white noise. Now, in generating discrete broadband white-noise samples from discrete random numbers Z_i with standard deviation σ_z, for any stationary process $X(t)$, the power spectrum of the nth derivative (written $X^{(n)}(t)$), satisfies the relationship $S_{X^{(n)}}(\omega) = (2\pi\omega)^{2n} S_X(\omega)$, where the constant (band-limited white noise) spectral level is $S_X = \sigma_Z^2$. Therefore, it follows that samples W_{b_i}, of a continuous band-limited process $W_b(t)$, constructed at discrete times t_i, can be obtained directly as

$$W_{b_i} = Z_i/\sqrt{\Delta t}. \tag{33}$$

Moreover, a process with the same *mean-square* properties as the derivative process $\dot{W}_{b_i}$, can be obtained directly from the discrete samples (of a surrogate process) as

$$\dot{W}_{b_i} \equiv \frac{\pi}{\sqrt{3}} Z_i/(\Delta t)^{3/2}, \tag{34}$$

where the $\equiv$ sign is used to indicate that these are only equivalent discrete processes in a mean square sense—autocovariance properties will however be different. Similarly, a process with the same mean square properties as the second derivative process $\ddot{W}_{b_i}$, can also be obtained directly from the discrete samples, namely,

$$\ddot{W}_{b_i} \equiv \frac{\pi^2}{\sqrt{5}} Z_i/(\Delta t)^{5/2}. \tag{35}$$

Therefore, the r.m.s. magnitude of the error based on one term in equation (25), assuming discrete random numbers for $Q(t) = W_b(t)$, and using equations (33) and (34), is

$$e_{1_{r.m.s.}} = \frac{\sigma_z(\Delta\tau)^{1/2}}{12\omega_d} \left| \frac{\pi^2}{3} (\sin \omega_d(t - t_0))^2 + (\omega_d \Delta\tau)^2 ((\cos \omega_d(t - t_0))^2 + 1) \right|^{1/2}. \tag{36}$$

The r.m.s. value of the standard trapezoidal approximation of the integral (first term in equation (23)) is

$$\mathrm{I}_{r.m.s.} = \sigma_z(\Delta\tau)^{1/2} \left[\frac{h(t - t_0)^2}{4} + h(t - (t_0 + \Delta\tau))^2 + h(t - (t_0 + 2\Delta\tau))^2 + \cdots + \frac{h(0)^2}{4} \right]^{1/2} \tag{37}$$

and therefore the particular form of r.m.s. ratio (26) is

$$r_{e_1} = \frac{1}{12\omega_d} \left[\frac{\left| \frac{\pi^2}{3} (\sin \omega_d(t - t_0))^2 + (\omega_d \Delta\tau)^2 [(\cos \omega_d(t - t_0))^2 + 1] \right|}{\frac{h(t - t_0)^2}{4} + h(t - (t_0 + \Delta\tau))^2 + h(t - (t_0 + 2\Delta\tau))^2 + \cdots + \frac{h(0)^2}{4}} \right]^{1/2}. \tag{38}$$

Figure 5(a) shows 20 simulated displacement sample functions of the integral in equation (21) for a system with a damped natural frequency $\omega_d = 1$ rad/s and $\xi = 10^{-6}$, driven by band-limited white noise obtained from the first term in equation (23), integrating from $t_0 = 0$ to arbitrary time t, shown as a function of the fraction of the oscillator-damped

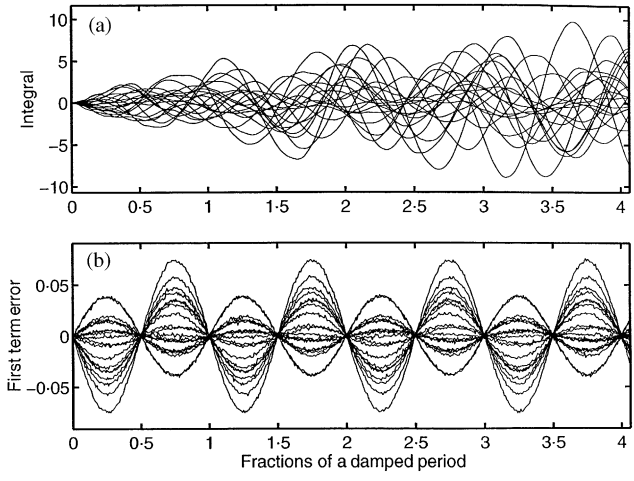

Figure 5. Simulated displacement ensemble for white-noise excitation. (a) Transition integral histories; (b) $O(\Delta\tau^2\Delta f')$ displacement truncation error histories.

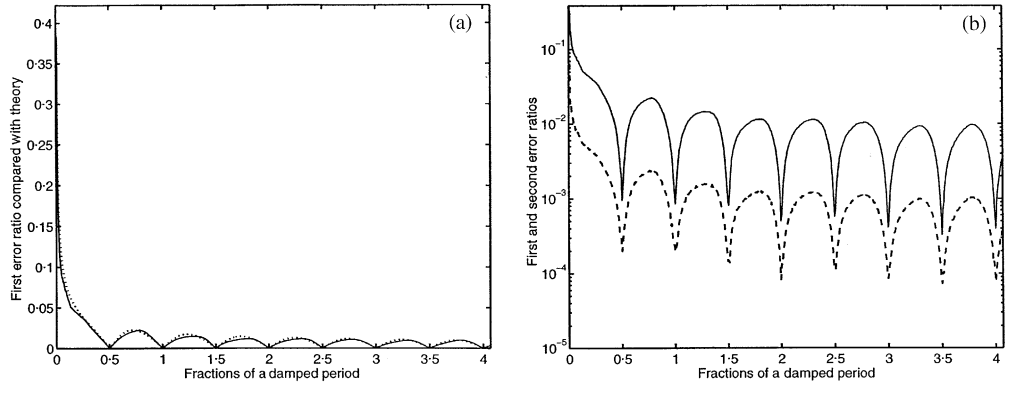

Figure 6. Truncation error ratios for displacement response to white-noise excitation. (a) Estimated $O(\Delta\tau^2\Delta f')$ error ratio compared with theory; (b) —, estimated $O(\Delta\tau^2\Delta f')$ and – – – –, $O(\Delta\tau^4\Delta f''')$ error ratios.

natural period $\omega_d(t - t_0)/(2\pi)$. The time step chosen is $\Delta\tau = 0{\cdot}05$ s. Figure 5(b) shows sample functions of the corresponding $O(\Delta\tau^2\Delta f')$ truncation error, obtained by using the first term in equation (25). Figure 6(a) shows the estimated r.m.s. ratio using the ensemble of error sample functions and integrals shown in Figures 5(a) and 5(b), compared to the theoretical relative integration error obtained by using equation (38). This comparison clearly shows that equation (38) gives a very good estimate of the $O(\Delta\tau^2\Delta f')$ error and therefore from the asymptotic series properties for equation (23), and also gives a practical upper bound on the total relative truncation error. Both theory and simulation also show two important things: first, that the largest relative error arising in the use of equation (23) occurs as $t - t_0 \to 0$, and second, that the relative error is a minimum for any integer multiple of the damped natural period, i.e., at $t - t_0 = k\pi/\omega_d$ for $k = 1, 2, \ldots$. These findings will be examined in detail in sections 4 and 5 respectively. Figure 6(b) shows the same relative truncation error in displacement, plotted on a log-scale and separated into its $O(\Delta\tau^2\Delta f')$ and $O(\Delta\tau^4\Delta f''')$ contributions. The initial implications of this are that any

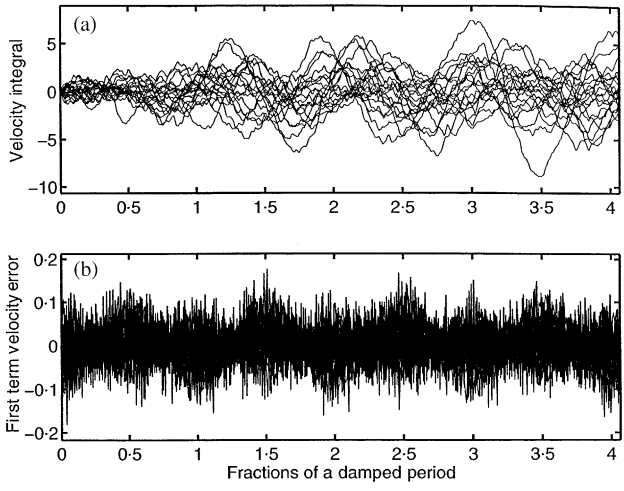

Figure 7. Simulated velocity ensemble for white noise excitation. (a) Velocity transition integral histories; (b) $O(\Delta\tau^2\Delta f')$ velocity truncation error histories.

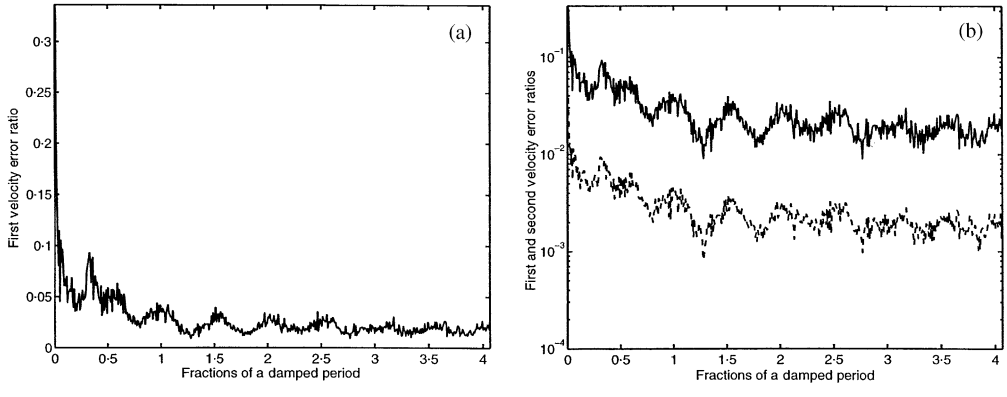

Figure 8. Truncation error ratios for velocity response to white-noise excitation. (a) Estimated $O(\Delta\tau^2\Delta f')$ error ratio; (b) —, estimated $O(\Delta\tau^2\Delta f')$ and – – – –, $O(\Delta\tau^4\Delta f''')$ velocity error ratios.

non-zero integer value of k would seem to be appropriate to ensure minimum $O(\Delta\tau^2\Delta f')$ error in equation (21) using standard trapezoidal integration. But there are two greater advantages derived from this choice, which can be identified when the velocity error is examined, and second, when the properties of the $O(\Delta\tau^2\Delta f')$ term are examined in detail. Before then, Figures 7(a), 7(b), 8(a) and 8(b) show velocity information similar to that shown in Figures 5(a)–6(b), resulting from the use of equation (22). Figure 7(b) in particular, shows that in integrating the velocity equation, there is no obvious preferred transition interval. Indeed, it would appear that unless the $O(\Delta\tau^2\Delta f')$ velocity error is removed, then a large velocity error will be propagated. As a matter of fact when $t - t_0 = k\pi/\omega_d$ for integer k, the ϕ_2 function in equation (5) is zero, so it is possible to obtain displacement transitions without the need to propagate velocity information. Equation (6) is therefore redundant. But the question then for broadband excitation is how large should the integer k be for acceptable errors in finite transitions, and second how is it possible, without velocity information, to generate accurate, *detailed* displacement histories within finite intervals

$(t_0 + k\pi/\omega_d) < t < (t_0 + (k+1)\pi/\omega_d)$. The second question will be addressed in section 7, but the first question will be answered in the following sections 4–6, by examining truncation errors for the categories defined at the beginning of this section, i.e., case (1), and special case (2) when transitions are integer multiples of the damped natural period.

4. TRUNCATION ERROR ANALYSIS FOR SINGLE-STEP TRANSITIONS OF LENGTH $\Delta\tau$

Figure 6(a) shows that as the transition interval $t - t_0 \to 0$ the displacement error ratio r_{e_1} (as predicted by equation (38)) grows to its worst case, i.e., a seemingly large value. Figure 8(a) also shows similar behaviour for the velocity integral. Both findings suggest that for trapezoidal integration of equations (5) and (6) with discrete band-limited white noise excitation, when a single transition interval is chosen equal to the integration step length $\Delta\tau$, there will be a convergence problem as $\Delta\tau \to 0$. This is case (1) as defined at the beginning of section 3, and the purpose of this section is to examine, for this case, the properties of the truncation error in more detail. This is approached by constructing both truncation error bounds and explicit relative r.m.s. estimates to confirm the rates of convergence in trapezoidal integration of equations (21) and (22). This may seemingly represent a slight digression from the development of an optimal integration scheme at the best transition interval (as completed in section 5), but it is important because it provides an alternative time-domain state-transition algorithm, against which propagation errors associated with multi-transitions can be compared in section 6.

In conventional trapezoidal integration with n steps of size $\Delta\tau$, error bounds are well known, i.e., given by the magnitude of the second derivative of the integrand within the interval $t_0 < \tau < t$, i.e.,

$$e_{upper} = \frac{n(\Delta\tau)^3}{12} \operatorname{Max} |\ddot{G}| \tag{39}$$

namely in terms of the second derivatives with respect to τ of the integrands G_1 and G_2 in equations (21) and (22). From equation (29), and the corresponding version for velocity, it follows that these second derivatives are

$$\ddot{G}_1(\tau) = \ddot{Q}(\tau) H_1(\tau) - 2\dot{Q}(\tau) \dot{H}_1(\tau) + Q(\tau) \ddot{H}_1(\tau), \tag{40}$$

$$\ddot{G}_2(\tau) = \ddot{Q}(\tau) H_2(\tau) - 2\dot{Q}(\tau) \dot{H}_2(\tau) + Q(\tau) \ddot{H}_2(\tau), \tag{41}$$

where

$$H_1(\tau) \equiv h(t - \tau) \tag{42}$$

and

$$H_2(\tau) \equiv \dot{h}(t - \tau). \tag{43}$$

Now for case (1) with $n = 1$, i.e., a single transition from t_0 to t, such that $\Delta\tau_2 = t - \tau$, then

$$\ddot{G}_1(\tau) = \ddot{Q}(\tau) h(\Delta\tau_2) - 2\dot{Q}(\tau) \dot{h}(\Delta\tau_2) + Q(\tau) \ddot{h}(\Delta\tau_2), \tag{44}$$

$$\ddot{G}_2(\tau) = \ddot{Q}(\tau) \dot{h}(\Delta\tau_2) - 2\dot{Q}(\tau) \ddot{h}(\Delta\tau_2) + Q(\tau) \dddot{h}(\Delta\tau_2), \tag{45}$$

where

$$\ddot{h}(t) = \frac{1}{(\rho_1 - \rho_2)} [\rho_1^2 \, e^{\rho_1 t} - \rho_2^2 \, e^{\rho_2 t}], \tag{46}$$

$$\dddot{h}(t) = \frac{1}{(\rho_1 - \rho_2)} [\rho_1^3 \, e^{\rho_1 t} - \rho_2^3 \, e^{\rho_2 t}]. \tag{47}$$

When the step size $\Delta\tau = t - t_0$, and the increment $\Delta\tau_2 = t - \tau$ always remains small, then first order approximations to the IRF (8) and its derivatives are appropriate, namely

$$h(\Delta\tau_2) = \Delta\tau_2 + O(\Delta\tau_2^2), \tag{48}$$

$$\dot{h}(\Delta\tau_2) = 1 + (\rho_1 + \rho_2)\,\Delta\tau_2 + O(\Delta\tau_2^2), \tag{49}$$

$$\ddot{h}(\Delta\tau_2) = (\rho_1 + \rho_2) + \left(\frac{\rho_1^3 - \rho_2^3}{\rho_1 - \rho_2}\right)\Delta\tau_2 + O(\Delta\tau_2^2), \tag{50}$$

$$\dddot{h}(\Delta\tau_2) = \frac{(\rho_1^3 - \rho_2^3)}{(\rho_1 - \rho_2)}\left(1 + \left(\frac{\rho_1^4 - \rho_2^4}{\rho_1^3 - \rho_2^3}\right)\Delta\tau_2\right) + O(\Delta\tau_2^2). \tag{51}$$

If $Q_i = W_{bi}$ from equations (33)–(35), then the magnitudes of the second derivatives appropriate for the integrands in equations (21) and (22) with integration time-step $\Delta\tau$ are maximized when $\Delta\tau_2 = \Delta\tau$, and therefore the errors are bounded by the inequalities

$$|\ddot{G}_1(\tau_i)| \leqslant \left|\frac{\pi^2}{\sqrt{5}} Z_{1i}(\Delta\tau)^{-3/2}\right| + \left| -\frac{\pi}{\sqrt{3}} Z_{2i}((\Delta\tau)^{-3/2} + (\rho_1 + \rho_2)\,\Delta\tau^{-1/2})\right| + \left|Z_{3i}\left[(\rho_1 + \rho_2)\,\Delta\tau^{-1/2} + \left(\frac{\rho_1^3 - \rho_2^3}{\rho_1 - \rho_2}\right)\Delta\tau^{1/2}\right]\right|, \tag{52}$$

$$|\ddot{G}_2(\tau_i)| \leqslant \left|\frac{\pi^2}{\sqrt{5}} Z_{1i}(\Delta\tau^{-5/2} + (\rho_1 + \rho_2)\,\Delta\tau^{-3/2})\right| + \left| -\frac{\pi}{\sqrt{3}} Z_{2i}\left((\rho_1 + \rho_2)\,\Delta\tau^{-3/2} + \left(\frac{\rho_1^3 - \rho_2^3}{\rho_1 - \rho_2}\right)\Delta\tau^{-1/2}\right)\right| + \left|Z_{3i}\left[\frac{(\rho_1^3 - \rho_2^3)}{(\rho_1 - \rho_2)}\left[\Delta\tau^{-1/2} + \left(\frac{\rho_1^4 - \rho_2^4}{\rho_1^3 - \rho_2^3}\right)\Delta\tau^{1/2}\right]\right|, \tag{53}$$

where a distinction has been made between the different discrete samples Z_{1i}, Z_{2i}, Z_{3i} of the same process Z_i occurring at discrete time τ_i. Now, since

$$\ddot{G}_1 = O(\Delta\tau^{-3/2}) \quad \text{and} \quad \ddot{G}_2 = O(\Delta\tau^{-5/2}), \tag{54, 55}$$

it can be seen that $\Delta\tau^{-3/2}$ and $\Delta\tau^{-5/2}$ terms dominate in $\ddot{G}_1(\tau_i)$ and $\ddot{G}_2(\tau_i)$; therefore for a single step $\Delta\tau$, good approximations to the upper bound (39) for each respective integration error are

$$e_{1_{upper}} \approx 0{\cdot}52\,\Delta\tau^{3/2} \max|Z_i|, \quad e_{2_{upper}} \approx 0{\cdot}37\,\Delta\tau^{1/2} \max|Z_i|. \tag{56, 57}$$

These estimates initially suggest that for a case (1) scheme, the absolute truncation error terms in both state transition equations (21) and (22) converge, but the velocity predictions via equation (6), converge at a much slower rate than the displacement predictions via

equation (5). However, if attention is focused on the displacement errors, the first summation in equation (37) for discrete band-limited white noise excitation reduces to

$$\mathrm{I}_{r.m.s.} \approx \frac{\sigma_Z(\Delta\tau)^{3/2}}{2}. \tag{58}$$

This term is of the same order as equation (56), and would suggest that for displacement prediction (in terms of relative truncation error), the scheme will never converge. Further support for this suggestion initially comes from the displacement r.m.s. error. Equation (26) can be used to obtain an explicit r.m.s. error ratio r_{e_1} for a single transition $t - t_0 = \Delta\tau$, i.e., equal to a single integration step of length $\Delta\tau$. Approximations (48) and (49) imply that $h(\Delta\tau) \approx \Delta\tau$ and $\dot{h}(\Delta\tau) \approx 1$, and by using equation (58), the special case of equation (32) simplifies to

$$e_1 = \frac{(\Delta\tau)^2}{12}\,[[h(0)\dot{Q}(t) - \dot{h}(0)Q(t)] - [h(\Delta\tau)\dot{Q}(t_0) - \dot{h}(\Delta\tau)Q(t_0)]], \tag{59}$$

which on using equations (33), (34), (48) and (49), gives an approximate r.m.s. value,

$$e_{1_{r.m.s.}} = \frac{\sigma_z(\Delta\tau)^{3/2}}{12}\left[2 + \frac{\pi^2}{3}\right]^{1/2} \tag{60}$$

and a corresponding special version of ratio (38)

$$r_{e_1} = \frac{1}{3\sqrt{2}}\left[1 + \frac{\pi^2}{6}\right]^{1/2} = 0{\cdot}384. \tag{61}$$

This result is confirmed in Figure 6(a) and shows more explicitly that for case (1) transitions, the displacement error ratio r_{e_1} for a band-limited (discrete) white-noise-driven oscillator, tends to a constant and is therefore independent both of step size $\Delta\tau$ and damped natural frequency ω_d. This adds further support to the suggestion that a simple recursive scheme using equations (5), (6), and the first term in equation (23), would never converge as $\Delta\tau \to 0$, since the r.m.s. value of the first order error term in equation (23) would not diminish faster than the r.m.s. of the two-term integral sum. Indeed, as $\Delta\tau \to 0$ the first order r.m.s. error could be expressed explicitly in terms of the sum r.m.s., namely $e_{r.m.s.} = 0{\cdot}384\mathrm{I}_{r.m.s.}$. This would seem to pose a serious limitation for case (1)-based integration. However, this is a mean square error analysis for single step integration over a single transition. A closer look at how the error propagates after many steps is more important—and for this, covariance information is needed. Some insight into the covariance properties of the displacement error can be obtained by writing equation (23) for $t - t_0 = \Delta\tau$, as

$$\mathrm{I} = \frac{(\Delta\tau)}{2}\,[f(t_0) + f(t)] - \frac{(\Delta\tau)^2}{12}\,[f'(t) - f'(t_0)] + O(\Delta\tau^4\Delta f'''), \tag{62}$$

which simplifies to

$$\mathrm{I} = \frac{(\Delta\tau)}{2}\,[h(\Delta\tau)\,Q(t_0)] - \frac{(\Delta\tau)^2}{12}\,[-\dot{h}(0)\,Q(t) - [h(\Delta\tau)\,\dot{Q}(t_0) - \dot{h}(\Delta\tau)\,Q(t_0)]] + O(\Delta\tau^4\Delta f'''), \tag{63}$$

and noting that

$$\dot{h}(0)\,Q(t) - \dot{h}(\Delta\tau)\,Q(t_0) \approx Q(t) - Q(t_0) \approx \dot{Q}(t_0)\,\Delta\tau \tag{64}$$

gives, upon using approximations (48) and (49) for h and $\dot{h}$,

$$\mathrm{I} \approx \frac{(\Delta\tau)^2}{2}\,[Q(t_0)] + \frac{(\Delta\tau)^3}{6}\,[\dot{Q}(t_0)] + O(\Delta\tau^4 \Delta f'''). \tag{65}$$

Equation (65) shows that the first error term in standard trapezoidal integration will actually behave in proportion to the derivative of the excitation process. Since the power spectrum of a derivative process will behave like ω^2, most of the energy in the error will be located at high frequency. Therefore, even though the r.m.s. value of the error may be relatively large, all of the "power" in the integration error, will be concentrated at high frequency, well above the system natural frequency. A similar conclusion can be reached for the velocity errors. The propagation of these errors over multiple transitions, can in fact be understood in terms of moving average filters, which have their own frequency response characteristic capable of error filtering. Therefore, error propagation over multiple tranistions will be examined in section 6 for both this scheme and the optimum scheme, described in section 5.

5. AN OPTIMUM FIXED-STEP INTEGRATION SCHEME

Turning attention now to the most important special case, where the transition interval is selected to be an integer multiple of the damped natural period $t - t_0 = k\pi/\omega_d$, it was identified in section 3 that for this case the ϕ_2 transition function in equation (5) is zero and hence transitions can be made without velocity information. This significantly reduces the computation required in each transition. But a more important realization is that the $O(\Delta\tau^2 \Delta f')$ truncation error can be *evaluated* with minimal effort. To explain and justify this, the integral in any finite transition $t - t_0$ can be estimated by using the first two terms of equation (23), i.e.,

$$\mathrm{I} = (\Delta\tau)\left[\frac{1}{2}\,f_1 + f_2 + \cdots + f_{N-1} + \frac{1}{2}\,f_N\right] - \frac{B_2(\Delta\tau)^2}{2!}\,[f'_N - f'_1] + O(\Delta\tau^4) \tag{66}$$

and noting from equations (27) and (28), in general, for arbitrary single transitions of multiple steps $\Delta\tau$, to evaluate the $O(\Delta\tau^2 \Delta f')$ truncation error, the differentiated excitation $\dot{Q}(t)$ is needed at each transition. In case (1) of section 4 for example, error reduction in both displacement and velocity integrals (5) and (6), is needed after each small transition. This would lead to a very costly computation involving numerical differentiation of a discrete random process—a highly undesirable operation. However, for the special case where the transition is $t - t_0 = k\pi/\omega_d$, since $h(0) = 0$ and $h(k\pi/\omega_d) = 0$, the transition integral in equation (5) can be obtained from

$$\mathrm{I}_{opt} = (\Delta\tau)\left[\frac{1}{2}\,f_1 + f_2 + \cdots + f_{N-1} + \frac{1}{2}\,f_N\right] - \frac{(\Delta\tau)^2}{12}\,[\dot{h}(k\pi/\omega_d)\,Q(t_0) - \dot{h}(0)\,Q(t)]$$
$$+ O(\Delta\tau^4 \Delta f'''). \tag{67}$$

Therefore, to evaluate the $O(\Delta\tau^2 \Delta f')$ term in equation (66), equation (67) shows the differentiation of the excitation is not required — only numerical values of the excitation at

the beginning, and end, of the transition. Since the transition $t - t_0$ will be many multiples of $\Delta\tau$ (possibly up to 1000 times), correction involves an insignificant amount of computation compared with the first summation. The asymptotic expansion properties of equation (23), enable the $O(\Delta\tau^4 \Delta f''')$ error to be obtained by using the numerical integration formula (67) as

$$e \approx \frac{(\Delta\tau)^4}{720} [f'''(t) - f'''(t_0)]. \tag{68}$$

This requires the third derivative for the excitation; consequently, only an approximate prediction of $O(\Delta\tau^4 \Delta f''')$ can in general be expected. However, it is now shown that by evaluating the leading $O(\Delta\tau^2 \Delta f')$ error term rather than eliminating it, this simple equal-weighted $O(\Delta\tau^4 \Delta f''')$ scheme has highest accuracy compared with all other orders. The basis for this assertion is achieved by writing the EMSF in the form

$$\mathrm{I}_{\Delta\tau} = (\Delta\tau)\left[\frac{1}{2} f_1 + f_2 + \cdots + f_{N-1} + \frac{1}{2} f_N\right] + O((\Delta\tau)^2 \Delta f') + O((\Delta\tau)^4 \Delta f''') + O((\Delta\tau)^6 \Delta f^{(5)}) + \cdots, \tag{69}$$

where the first three error terms are written explicitly in the form $O((\Delta\tau)^2 \Delta f') = -[(\Delta\tau)^2/12][f'_N - f'_1]$, $O((\Delta\tau)^4 \Delta f''') = [(\Delta\tau)^4/720](f_N^{(3)} - f_1^{(3)})$ and $O((\Delta\tau)^6 \Delta f^{(5)}) = -[(\Delta\tau)^6/(42 \times 720)](f_N^{(5)} - f_1^{(5)})$. Now, by using equation (69), Simpson's rule can be generated by writing down $\mathrm{I}_{(2\Delta\tau)}$ in terms of alternate ordinates and then by eliminating the $O(\Delta\tau^2 \Delta f')$ term: i.e.,

$$\mathrm{I}_{2\Delta\tau} = 2\Delta\tau\left[\frac{1}{2} f_1 + f_3 + \cdots + f_{N-2} + \frac{1}{2} f_N\right] + 4O((\Delta\tau)^2 \Delta f') + 16O((\Delta\tau)^4 \Delta f''') + 64O((\Delta\tau)^6 \Delta f^{(5)}) + \cdots, \tag{70}$$

and, by using equations (69) and (70), the integral can be written as

$$\mathrm{I}_S = \frac{1}{3}(4\mathrm{I}_{\Delta\tau} - \mathrm{I}_{2\Delta\tau}) = \frac{\Delta\tau}{3}[f_1 + 4f_2 + 2f_3 + \cdots + 4f_{N-1} + f_N] - 4O((\Delta\tau)^4 \Delta f''') - 20O((\Delta\tau)^6 \Delta f^{(5)}) + \cdots, \tag{71}$$

i.e., the usual 1-4-2-4-$\cdots$ Simpson's rule. The $O(\Delta\tau^4 \Delta f''')$ scheme I_{opt} given by equation (67), can actually be combined with Simpson's rule to eliminate the leading $O(\Delta\tau^4 \Delta f''')$ term, to create the following $O(\Delta\tau^6 \Delta f^{(5)})$ scheme:

$$\mathrm{I}_6 = \frac{1}{5}(4\mathrm{I}_{opt} + \mathrm{I}_S) = \frac{(\Delta\tau)}{15}[7f_1 + 16f_2 + 14f_3 + \cdots + 16f_{N-1} + 7f_N] - \frac{4}{5} \times \frac{(\Delta\tau)^2}{12}[\dot{h}(k\pi/\omega_d) Q(t_0) - \dot{h}(0) Q(t)] - \frac{16}{5} O((\Delta\tau)^6 \Delta f^{(5)}) + \cdots. \tag{72}$$

Since "higher order", does not necessarily translate into higher accuracy, the question for discrete random excitation is, which of the four possibilities will always be most accurate, namely when (1) equation (66) is used with an arbitrary transition, as opposed to

a transition equal to an integer multiple of the damped period, without the $O(\Delta\tau^2\Delta f')$ term being evaluated, (2) equation (67) is used for a transition equal to an integer multiple of the damped period, i.e., where the $O(\Delta\tau^2\Delta f')$ term is evaluated, (3) Simpson's rule (equation (71)) is used, and (4) the $O(\Delta\tau^6\Delta f^{(5)})$ scheme (equation (72)) is used.

These questions can be answered definitively first by using equations (28–30) for the derivatives needed in the leading error terms in the EMSF equation (23). Now at transitions equal to an integer multiple of the damped period, $h(0) = h(k\pi/\omega_d) = 0$ and $\dot{h}(0) = \dot{h}(k\pi/\omega_d) \approx 1$, the corresponding derivative terms will be dominated by the magnitude of $\mathrm{d}^{(n-1)}Q/\mathrm{d}t^{n-1}$. Then by using equations (33–35) and noting that $\mathrm{d}^4Q/\mathrm{d}t^4 \equiv (\pi^4/\sqrt{9})[Z_i/(\Delta\tau)^{9/2}]$, the r.m.s. error terms will be closely approximated by

$$e_{\substack{\Delta\tau^2 \\ r.m.s.}} = \frac{\sqrt{2}}{12}\,\sigma_z\Delta\tau^{3/2}, \quad e_{\substack{\Delta\tau^4 \\ r.m.s.}} = \sqrt{\frac{2}{5}}\times\frac{3\pi^2}{720}\,\sigma_z\Delta\tau^{3/2}, \quad e_{\substack{\Delta\tau^6 \\ r.m.s.}} = \sqrt{\frac{2}{9}}\times\frac{5\pi^4}{42\times720}\,\sigma_z\Delta\tau^{3/2} \tag{73a–c}$$

and from the summation in equation (37) for $\xi_k = 0$, $\mathrm{I}_{r.m.s.} = \sigma_z\sqrt{k\pi}\omega_d^{-3/2}$ (where k refers to integer or quarter fractions of the damped period), the r.m.s. ratios corresponding to equation (38) will be

$$r_{\Delta\tau^2} = \sqrt{\frac{2}{k}}\times\frac{\pi^{-1/2}}{12}\,(\omega_d\Delta\tau)^{3/2}, \quad r_{\Delta\tau^4} = \sqrt{\frac{2}{5k}}\times\frac{3\pi^{3/2}}{720}\,(\omega_d\Delta\tau)^{3/2},$$

$$r_{\Delta\tau^6} = \sqrt{\frac{2}{9k}}\,\frac{5\pi^{7/2}}{(42\times720)}\,(\omega_d\Delta\tau)^{3/2}\cdots \tag{74a–c}$$

where the suffices $(\Delta\tau)^2$, $(\Delta\tau)^4$, and $(\Delta\tau)^6$ in equation (74) correspond for simplicity to the $O((\Delta\tau)^2\Delta f')$, $O((\Delta\tau)^4\Delta f''')$, and $O((\Delta\tau)^6\Delta f^{(5)})$ terms respectively. When the transition is equal to an integer multiple of the damped period, then

$$[e_{\Delta\tau^2}/e_{\Delta\tau^4}]_{r.m.s.} = 4{\cdot}53, \tag{75}$$

and

$$\left[\frac{e_{\Delta\tau^4}}{e_{\Delta\tau^6}}\right]_{r.m.s.} = 3{\cdot}42 \tag{76}$$

independently of $\Delta\tau$ and ω_d. By contrast, for an arbitrary transition, the derivative terms in equations (28–30) will be maximized when leading terms $h(t-\tau)(\mathrm{d}^nQ/\mathrm{d}t^n)$ are dominant: i.e., when $(t - t_0) = 2k\pi/\omega_d$ for $k = \frac{3}{4}$, $k = \frac{7}{4}$, etc. Therefore, an estimate for the worst case for ratio equation (38), is

$$\underset{\dot{\mathrm{Q}}\ dominant}{r_1} = \frac{\sqrt{2\pi\omega_d\Delta\tau}}{18}. \tag{77}$$

To give some intermediate confirmation of these ratios for transitions equal to an integer multiple of the damped period, with $\sigma_z = 1$, $\Delta t = 0{\cdot}05$, $\omega_d = 1$ rad/s and $k = 1$ for example, the first two ratio estimates give $r_{\Delta\tau^2} = 7{\cdot}43\times10^{-4}$ and $r_{\Delta\tau^4} = 1{\cdot}64\times10^{-4}$, in very close agreement with Figure 6(a). The value for the third ratio is $r_{\Delta\tau^6} = 4{\cdot}79\times10^{-5}$. For the same parameters, $\underset{\dot{\mathrm{Q}}\ dominant}{r_1} = 0{\cdot}022$ after $\frac{3}{4}$ of the first cycle, as predicted in Figure 6(a) and again shows very good agreement with the estimated value. Now, the answer to question (1) posed

earlier can be obtained from equations (74a) and (77) for the first cycle, which gives the ratio $r_{1\ \dot{Q}\ dominant} / r_{1\ Q\ dominant} = \sqrt{2}\pi/3\omega_d \Delta\tau$. Since in any integration involving N steps per cycle, increasingly small $\Delta\tau$ must be chosen as ω_d increases, and since the damped period $T = 2\pi/\omega_d$, and $T/\Delta\tau = 2\pi/\omega_d\Delta\tau = N \gg 1$, then $r_{1\ \dot{Q}\ dominant} / r_{1\ Q\ dominant} = N/3$. The typical range is is $50 < N < 1000$, depending on the required bandwidth (as discussed in section 2). Therefore under general conditions $r_{1\ \dot{Q}\ dominant} \gg r_{1\ Q\ dominant}$ confirming that equation (69) used with a transition interval is equal to an integer multiple of the period, will always give lower truncation error than for an arbitrary transition. The answer to question (2) is given by equation (75) at a transition equal to an integer multiple of the period. Evaluation of the leading $O(\Delta\tau^2 \Delta f')$ will always reduce the error to the leading $O(\Delta\tau^4 \Delta f''')$ term, which is always smaller by a factor $= 4{\cdot}53$. The answer to question (3) is that at the optimal interval, Simpson's rule will increase the $O(\Delta\tau^4 \Delta f''')$ error by a factor of four times, and the $O(\Delta\tau^6 \Delta f^{(5)})$ error by a factor of 20 times, that of equation (69). The elimination of the $O(\Delta\tau^2 \Delta f')$ error term used to create Simpson's rule is therefore of no benefit, because the $O(\Delta\tau^4 \Delta f''')$ error has been increased to the same magnitude of the term eliminated. Finally, the answer to question (4) is that use of the $O(\Delta\tau^6 \Delta f^{(5)})$ scheme suggested by equation (72) would be of no benefit because the $O(\Delta\tau^6 \Delta f^{(5)})$ error would be increased by a factor of 16/5, which according to equation (76), would make this term as large as the $O(\Delta\tau^4 \Delta f''')$ error term that has been eliminated and would therefore be of no benefit either. The conclusion then is that the simplest scheme equation (67) in which the $O(\Delta\tau^2 \Delta f')$ term is evaluated, is optimal in the sense of having maximum accuracy for minimum computational effort. In summary, for a single transition integration, the overall error reduction obtained when using equation (67) as opposed to arbitrary trapezoidal integration, is given by the ratio $r_{1\ \dot{Q}\ dominant} / r_{(\Delta\tau)^4} = 10\sqrt{10}N/\pi^2 = 3{\cdot}2N$. This ratio varies between 150 and 3000 depending on bandwidth requirements. Figure 6(b), for example, shows this ratio is well over 100.

6. TRUNCATION ERROR PROPAGATION IN MULTIPLE TRANSITIONS

For the case (1) scheme of section 4, involving single transitions with single step integrations, it has been shown that explicit estimates of the local $O(\Delta\tau^2 \Delta f')$ and $O(\Delta\tau^4 \Delta f''')$ errors, can in principle be obtained directly by using both terms in equation (25). By contrast, for the special scheme of section 5, involving single transitions equal to an integer multiple of the damped natural period, the $O(\Delta\tau^4 \Delta f''')$ truncation error in equation (67), can be approximated from equation (68). Interest now focuses on using these error estimates to obtain explicit global truncation errors after many transitions. Error propagation for these two cases can be examined by writing the explicit state-transition equation (4) as a linear difference equation

$$\underline{x}_N(t) = A\underline{x}_{N-1} + \underline{I}_{N-1}, \tag{78}$$

where $\underline{x}_N(t)$, is the state vector after N transitions, A is the 2×2 state transition matrix, and $\underline{I}_{N-1}$ is the contribution to the integral at the Nth step. By introducing a truncation error at each step, equation (78) can be augmented and written explicitly as

$$\underline{x}_N(t) + \underline{\varepsilon}_{\underline{x}_N} = A^{N-1}(\underline{I}_0 + \underline{\varepsilon}_0) + A^{N-2}(\underline{I}_1 + \underline{\varepsilon}_1) + \cdots + (\underline{I}_{N-1} + \underline{\varepsilon}_{N-1}), \tag{79}$$

where $\underline{\varepsilon}_{N-1}$ is the Nth step truncation error and $\underline{\varepsilon}_{\underline{x}_N}$ is the propagated truncation error in the state vector. The initial state has for simplicity been assumed to be zero. Linearity allows

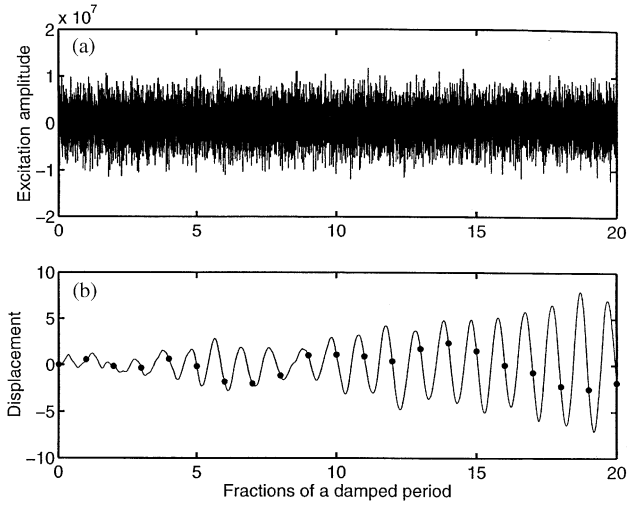

Figure 9. White-noise-driven oscillator. (a) Excitation; (b) response via single-step transition method —, compared with the use of optimum $O(\Delta\tau^4\Delta f'''')$ integration scheme "·".

$\underline{\varepsilon}_{\underline{x}_N}$ to be written explicitly as

$$\underline{\varepsilon}_{\underline{x}_N} = A^{N-1}\underline{\varepsilon}_0 + A^{N-2}\underline{\varepsilon}_1 + \cdots + \underline{\varepsilon}_{N-1}. \tag{80}$$

Since equation (80) is a moving average filter, with discrete dynamic properties exactly the same as the oscillator, error propagation depends on the frequency content of the error process $\underline{\varepsilon}_{N-1}$. In other words, error energy well removed from resonance will be filtered out and will not propagate. This is precisely what is expected to happen for short duration transitions equal to the trapezoidal step size $\Delta\tau$ as predicted by equation (65). Now for finite duration transitions, the per-step errors can be broken down by using equation (25) in first order, second order terms, etc., and studied by using equation (80). Here, both first and second order error propagation are considered, but to generate the error terms in equation (23), it is necessary to obtain first, second, and third derivatives of the discrete excitation process, namely $\dot{Q}$, $\ddot{Q}$, and $\dddot{Q}$, as required from equations (28)–(30) at respective transition times $\tau = t_0$ and t for the two specific cases (1) $t - t_0 = k\pi/\omega_d$ and (2) $t - t_0 = \Delta\tau$. These differentials can be obtained in the frequency domain by using FFT. Figure 9(a) shows a discrete white noise excitation history applied to an oscillator with undamped natural frequency of 100 Hz and 0·1% critical damping. In Figure 9(b), 20 cycles of displacement are shown which have been predicted via a case (1) recursive scheme (i.e., equations (5) and (6) using standard trapezoidal integration) with transition length $t - t_0 = \Delta\tau = 9{\cdot}7656 \times 10^{-6}$ s, compared with a special case (2) scheme, using equation (67) with the same $\Delta\tau$ predicting at discrete times equal to multiples of the damped period, shown by a "·" symbol. Figure 10(a) shows total oscillator energy, and Figure 10(b) shows the magnitudes of the $O(\Delta\tau^2\Delta f')$ plus $O(\Delta\tau^4\Delta f''')$ error terms for case (1) and the $O(\Delta\tau^4\Delta f''')$ error for special case (2) both normalized by the total energy, corresponding to the information in Figure 9(b). Figure 11(a) shows a discrete white noise history and Figure 11(b) a history of the corresponding derivative (obtained in the frequency domain via FFT). Figure 11(c) shows displacement information similar to Figure 9(b), but for derivative white noise excitation. Figures 12(a) and 12(b) show corresponding energy and normalized errors.

Focusing on the error prediction in Figures 10(b) and 12(b), these confirm that the displacement errors obtained by using equation (67) are orders of magnitude smaller than

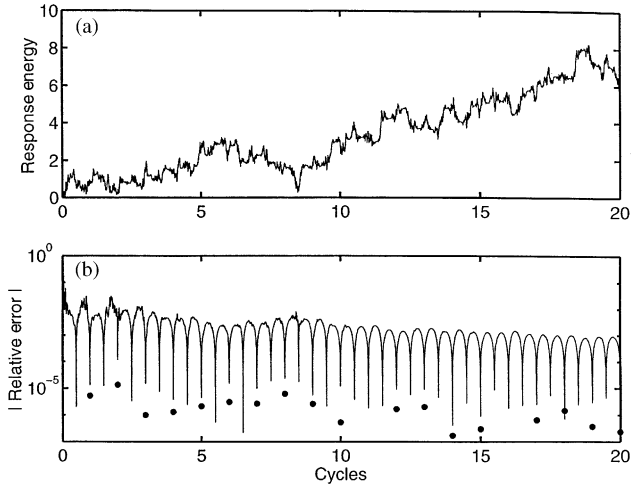

Figure 10. White-noise-driven oscillator. (a) Energy envelope; (b) absolute relative error for single-step transition method—, compared with optimum $O(\Delta\tau^4\Delta f'''')$ integration scheme "·".

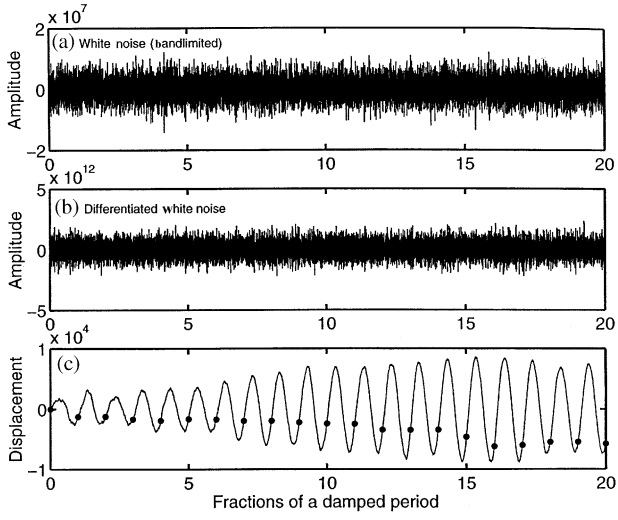

Figure 11. Differentiated white-noise-driven oscillator. (a) Original excitation; (b) excitation after differentiation; (c) response via single-step transition method —, compared with the use of optimum $O(\Delta\tau^4\Delta f'''')$ integration scheme "·".

the errors obtained from the case (1) scheme, for either band-limited discrete white noise, or the much more computationally problematic derivative white noise. The CPU time required for the case (1) scheme is several 100 times that required for equation (67). This shows that even for extremely non-smooth band-limited excitation, it is possible to predict displacement very accurately at discrete time equal to a damped natural period. However, a way has to be found to efficiently obtain the detailed displacement between these points at very fine discrete time steps $\Delta\tau$. This detailed information is now approached by using a Chebychev polynomial solution to equation (2).

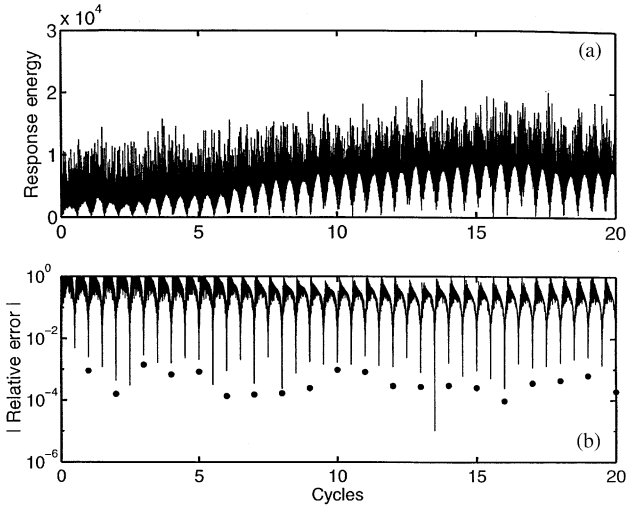

Figure 12. Differentiated white-noise-driven oscillator. (a) Energy envelope; (b) absolute relative error for single-step transition method —, compared with optimum $O(\Delta\tau^4\Delta f'''')$ integration scheme "·".

7. SINGLE-CYCLE SOLUTION VIA CHEBYCHEV POLYNOMIAL APPROXIMATION

Equation (67) using just a single sweep integration can be used to efficiently generate a vector of accurate displacements $\underline{q_\alpha}$, at integer multiples of the oscillator period say at a vector of discrete times $\underline{t_\alpha}$. By shifting the time axis and starting the integration (with zero-padding) a fraction of a cycle early, it is also possible to use the same equation to obtain a sequence of accurate displacements $\underline{q_\beta}$ at discrete time vector $\underline{t_\beta}$. The question is how can this be used to generate the detailed solution from the discrete values of the excitation? To do this, a Chebychev boundary-value solution of equation (2) can be exploited to give the detailed solution for any one cycle at any of the times in $\underline{t_\alpha}$. This has the advantage that the convergence criterion can be based on point values of the coefficients. A Chebychev polynomial approximation [37] to a continuous function is possible on the interval $[-1, 1]$ using the orthogonality property of Chebychev polynomials $\mathrm{T}_n(t) = \cos(n \arccos(t))$ in the form

$$q(t) = \sum_{k=1}^{m} c_k \mathrm{T}_{k-1}(t) - c_1/2, \tag{81}$$

where the continuous form of the orthogonality condition is

$$\int_{-1}^{1} \frac{\mathrm{T}_i(t)\mathrm{T}_j(t)}{\sqrt{1-t^2}}\,\mathrm{d}t = \begin{cases} 0 & \text{if } i \neq j, \\ \pi/2 & \text{if } i = j \neq 0, \\ \pi & \text{if } i = j = 0. \end{cases} \tag{82}$$

Chebychev polynomials also satisfy the recurrence relationship $\mathrm{T}_{n+1}(t) = 2t\mathrm{T}_n(t) - \mathrm{T}_{n-1}(t)$ for $n \geqslant 1$ giving $\mathrm{T}_0(t) = 1$, $\mathrm{T}_1(t) = t$, $\mathrm{T}_2(t) = 2t^2 - 1$, $\mathrm{T}_3(t) = 4t^3 - 3t$, etc. The coefficients c_k are usually rapidly decreasing, and the error, which is spread out over $[-1, 1]$, is dominated by the magnitude of the term $c_{m+1}\mathrm{T}_m(t)$. Since $|\mathrm{T}_m(t)| \leqslant 1$, the error is indicated

by the magnitude of the coefficient c_{m+1}. This feature allows an adaptive solution to be generated as explained shortly. The Chebychev polynomial expansions of the first derivative of a continuous function can be expressed directly in terms of the expansion of the function, namely

$$\dot{q}(t) = \sum_{k=1}^{m-1} c'_k \mathrm{T}_{k-1}(t) - c'_1/2, \tag{83}$$

where the coefficients c'_k of the first derivative can be obtained from the coefficients c_k by using the relationship

$$c'_{i-1} = c'_{i+1} + 2(i-1)\,c_i, \tag{84}$$

subject to initial condition $c'_{m+1} = c'_m = 0$, where $i = m, m-1, \ldots, 2$. Similarly, the second derivative can be expressed in the form

$$\ddot{q}(t) = \sum_{k=1}^{m-2} c''_k \mathrm{T}_{k-1}(t) - c''_1/2 \tag{85}$$

with a similar coefficient relationship,

$$c''_{i-1} = c''_{i+1} + 2(i-1)\,c'_i. \tag{86}$$

To construct a Chebychev polynomial expansion of any function over an arbitrary interval $[a, b]$, the linear transformation to non-dimensional time, i.e.,

$$t' = \frac{t - \frac{1}{2}(b+a)}{\frac{1}{2}(b-a)} \tag{87}$$

converts the interval from $[a, b]$ to $[-1, 1]$. Equation (2) therefore transforms to

$$\frac{\ddot{q}_k}{\mathrm{T}^2_{M/2}} + 2\xi_k\omega_{nk}\frac{\dot{q}_k}{\mathrm{T}_{M/2}} + \omega^2_{nk}q_k = Q(t'), \tag{88}$$

where $\mathrm{T}_{M/2} = \frac{1}{2}(b-a)$, i.e., the half-period. The coefficient relationships (84) and (86) can be written in matrix form as

$$\underline{c'} = A_1\underline{c'} + B_1\underline{c} \quad \text{and} \quad \underline{c''} = A_2\underline{c''} + B_2\underline{c'}, \tag{89, 90}$$

where square matrices A_1, B_1, A_2, and B_2 of dimension $n \times n$, are, wherever necessary, appropriately zero-padded. Equations (89) and (90) can be solved explicitly to give

$$\underline{c'} = (I - A_1)^{-1}B_1\underline{c} = G_1\underline{c} \tag{91}$$

and

$$\underline{c''} = (I - A_2)^{-1}B_2\underline{c'} = G_2\underline{c'} = G_1G_2\underline{c}. \tag{92}$$

Substitution of equations (81), (83) and (85) into equation (88) gives

$$\sum c_k'' \frac{\mathrm{T}_{k-1}}{\mathrm{T}_{M/2}^2} + 2\xi_k\omega_{nk} \sum c_k' \frac{\mathrm{T}_{k-1}}{\mathrm{T}_{M/2}} + \omega_{nk}^2 \sum c_k \mathrm{T}_{k-1}$$

$$-\frac{1}{2}\left[\frac{c_1''}{\mathrm{T}_{M/2}^2} + 2\xi_k\omega_{nk}\frac{c_1'}{\mathrm{T}_{M/2}} + \omega_{nk}^2 c_1\right] = Q(t'). \tag{93}$$

When equation (93) is multiplied by $\mathrm{T}_j(t')$ and integrated between -1 and $+1$, the orthogonality property (82) gives

$$\underline{c} = H^{-1}\underline{\mathrm{I}}_{\mathrm{Q}} \tag{94}$$

where

$$H = (\pi/2)\,[G_1G_2 + 2\xi_k\omega_{nk}G_1 + \omega_{nk}^2\mathrm{I}] \tag{95}$$

and

$$\mathrm{I}_{Q_j} = \int_{-1}^{1} \frac{Q(t)\mathrm{T}_j(t)}{\sqrt{1-t^2}}\,\mathrm{d}t. \tag{96}$$

To obtain a unique solution for the coefficient vector $\underline{c}$ for forced modal equation (2) satisfying boundary conditions $q(t_{\alpha_i}') = q_{\alpha_i}$ and $q(t_{\beta_i}') = q_{\beta_i}$, it is required that the bottom two rows of matrix H be replaced by the equations

$$\sum_{k=1}^{m} c_k\mathrm{T}_{k-1}(t_{\alpha_i}') - c_1/2 = q_{\alpha_i} \tag{97}$$

and

$$\sum_{k=1}^{m} c_k\mathrm{T}_{k-1}(t_{\beta_i}') - c_1/2 = q_{\beta_i}. \tag{98}$$

Now, to create an adaptive scheme, it is necessary to obtain the inverse matrix H^{-1} and vector $\underline{\mathrm{I}}_{\mathrm{Q}}$ for increasing values of n until the coefficient vector $\underline{c}$ converges in some sense. Inverse matrices H^{-1}, of increasing dimension, are needed for many possible values of n. Provided the half-period $\mathrm{T}_{M/2}$ does not change from cycle to cycle, an entire family of increasing dimension inverse H^{-1}, can be obtained in advance (say up to order 50). Once stored, this family need not be computed again. Evaluation of the improper integrals $\underline{\mathrm{I}}_{\mathrm{Q}}$ can be obtained by substitution of variable $t' = \sin(u)$, giving

$$\mathrm{I}_{\mathrm{Q}_j} = \int_{-\pi/2}^{\pi/2} Q(u)\,\mathrm{T}_j(u)\,\mathrm{d}u \tag{99}$$

in which the excitation function is known only at non-equispaced discrete times $u_i = \arcsin(t_i')$. This integral can be conveniently obtained by using a trapezoidal scheme of the form

$$\mathrm{I}_{Q_j} = \frac{h_1}{2}\,[Q(u_1)\mathrm{T}_j(u_1) + Q(u_2)\mathrm{T}_j(u_2)] + \frac{h_2}{2}\,[Q(u_2)\mathrm{T}_j(u_2) + Q(u_3)\mathrm{T}_j(u_3)] + \cdots, \tag{100}$$

in which the intervals are $h_1 = u_2 - u_1$, $h_2 = u_3 - u_2, \ldots$, etc.

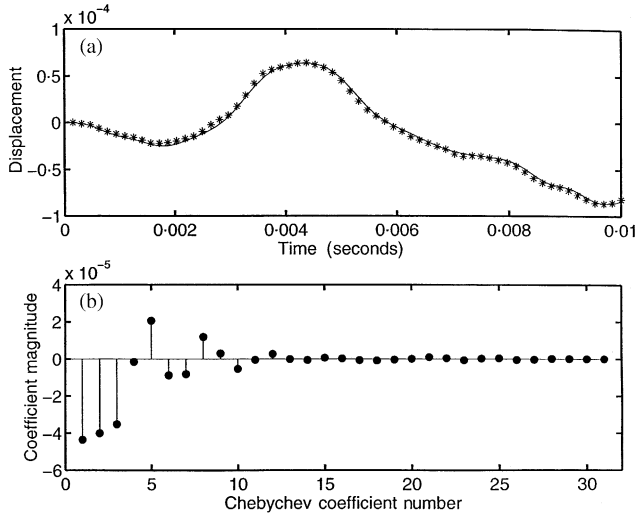

Figure 13. Chebychev polynomial solution for white-noise-driven oscillator. (a) Comparison with harmonic sum-based Laplace solution; (b) Chebychev coefficient magnitude.

The choice of boundary values needed to obtain a unique solution is not entirely arbitrary, although the first boundary is sensibly chosen as the local origin—i.e., the start of a cycle. The second boundary can in principle be chosen at any non-integer multiple of a damped period (since near an integer multiple, ill conditioning occurs). For convenience, the second boundary is best chosen at $\frac{3}{4}$ period. To create an adaptive boundary value Chebychev polynomial solution, a suitable convergence criterion then needs to be applied to terminate the generation of the varying dimension coefficient vector $\underline{c}$ at some value $k = n$. There are many practical possibilities here, for example, termination could be based on the condition that $\varepsilon_{n1} < e_{crit}$, where the magnitude of the relative error term is

$$\varepsilon_{n1} = |c_n|/\max|\underline{c}| \tag{101}$$

and e_{crit} is an acceptably small relative error criterion, say 10^{-4}. Unfortunately, this criterion does not easily account for correlation between successive coefficients. A better definition of the relative error term (and one that will be used shortly) is

$$\varepsilon_{n2} = \max[|c_n|, |c_{n+1}|]/\max[|\underline{c}| + \delta_e] \tag{102}$$

in which adjacent pairs of coefficients are used to construct the error, where a very small additive term, say $\delta_e = 10^{-40}$, is used to prevent degeneration when successive coefficients are precisely zero. Figure 13(a) shows, for discrete white noise excitation with 6·4 kHz bandwidth, a comparison between the response of an oscillator obtained via Chebychev polynomial BV solution compared with a fast Laplace solution using equation (16). The oscillator has 1% critical damping and 100 Hz natural frequency, for which one cycle is shown. The Chebychev polynomial boundary values were specified at $t = 0$ and $t = \frac{3}{4}T_M$ and, with a relative error criterion of 0·1%, convergence occurred for a polynomial of degree = 31. Figure 13(b) shows the convergence of the polynomial coefficients where it can be seen that there is some degree of correlation between adjacent coefficients, justifying the use of criterion (102).

8. ALGORITHM SUMMARY AND APPLICATIONS TO DISCRETE-TIME FORCING

Using the developments in sections 3–5, the fast state-transition algorithm for linear oscillators driven with general—or high bandwidth discrete random forcing, can now be summarized and applied. In particular, just two sweeps of displacement transition equation (5), integrated via equation (67), can generate the required boundary conditions needed for an adaptive Chebychev polynomial solution of section 7. In this section, the overall scheme is summarized in three detailed steps, and it is mentioned as to how this scheme can be used to obtain the displacement response of an m.d.o.f. normal mode system. The scheme is then applied to two s.d.o.f. cases, first to intermittent random excitation with quiet periods, and second to the prediction of far-future displacement histories for a long simulation. The efficiency of the scheme in these applications is compared with the Laplace/IFFT solution.

8.1. A DETAILED DESCRIPTION OF THE TWO-STAGE ALGORITHM

Step 1: A vector of accurate displacements $\underline{q}_\alpha$ is obtained by using state transition equation (5), at the times in discrete vector $\underline{t}_\alpha$, where $t_{\alpha_{i+1}} - t_{\alpha_i} = n_i\pi/\omega_d$, and where the integers n_i are chosen to give the desired successive multiples of the damped oscillator period. In these transitions, the function $\phi_2(t - t_0) = 0$, so the velocity transition equation (6) is not needed. Equation (5) is integrated using the $O(\Delta\tau^4\Delta f''')$ scheme equation (67) in the form

$$q(t_{\alpha_{i+1}}) = q(t_{\alpha_i}) + (\Delta\tau)(h(t_{\alpha_{i+1}} - (t_{\alpha i} + \Delta\tau))\,Q(t_{\alpha_i} + \Delta\tau) + h(t_{\alpha_{i+1}} - (t_{\alpha i} + 2\Delta\tau))\,Q(t_{\alpha_i} + 2\Delta\tau) + \cdots)$$

$$- \frac{(\Delta\tau)^2}{12}\,[\dot{h}(n_i\pi/\omega_d)\,Q(t_{\alpha_i}) - \dot{h}(0)\,Q(t_{\alpha_{i+1}})] + O(\Delta\tau^4\Delta f'''). \tag{103}$$

Step 2: By shifting the time-axis back by $\frac{1}{4}$ period, to define a new vector of discrete times $\underline{t}_\beta = \underline{t}_\alpha - \pi/2\omega_d$, a second (phased) vector of accurate displacements $\underline{q}_\beta$ is obtained at $\underline{t}_\beta$ by using exactly the same approach as Step 1 to predict all but the first value of displacement. This first (shifted-time) displacement, is predicted at the first $\frac{3}{4}$ period, using the Laplace/IFFT solution (via equation (16)), to avoid the significant numerical integration error which stems from the introduction of the sudden step at the origin, as a result of the time-shift. The same initial conditions at the origin are used in this one-off first-cycle Laplace solution, but in general, the excitation needs to be zero-padded both one cycle before- and one cycle after, as described in section 2.3. Subsequent displacements at all other times in $\underline{t}_\beta$ are predicted using an appropriate form of equation (103).

Step 3: At selected times $\underline{t}_{\alpha_i}$, a single cycle of continuous displacement response is obtained via a Chebychev BV solution using the corresponding elements of $\underline{q}_\alpha$ and $\underline{q}_\beta$ as boundary values, at times separated by $\frac{3}{4}$ of a damped period, the Chebychev polynomial solution is obtained via a coefficient vector $\underline{c}$ using equation (94), and the adaptive convergence criterion (102). To exploit quiet periods in intermittent excitation, greater efficiency can be obtained by switching from the use of a single-cycle Chebychev solution, to the unforced version of equation (5), when it is clear that a forced solution is not needed. To establish the conditions where this switch can be made, the magnitude of the largest value in a section of the excitation could in principle be used, but this can be problematic, since to confirm the importance of very small magnitudes, the forced solution is needed. An alternative criterion is to use the first two integrals in equation (96) to establish whether the excitation is effectively zero. In random forcing, for example, it would be very unlikely that

a non-zero section of excitation would be simultaneously orthogonal to both the first and second degree Chebychev polynomials.

Before applying the two-stage scheme to s.d.o.f. systems with intermittent excitation and for far-future transient displacement prediction, it should be mentioned that the scheme can be applied to m.d.o.f. normal mode systems, by solving in modal co-ordinates and then transforming back to physical co-ordinates. However, in a discrete solution, the physical excitation functions are usually generated (or sampled, in the case of experimental data) at common discrete times, such that the corresponding modal excitation vectors are also at the same common discrete times. However, because the different damped natural periods for each mode would not correspond exactly to an integer multiple of the sample step size there would be small misalignment at the end points. If the sampling rate for a high frequency mode were relatively low, then this indeed would create a problem. But as shown in section 2, in general, the sampling rate for transient response prediction has to be high anyway, such that the number of points N per cycle, would be in the region 50–1000, depending on the excitation spectrum. Consequently, this misalignment will be extremely small such that the nearest neighbourhood value in equation (103) could be used for the phased displacement predictions, especially when the transition interval $t_{\alpha_{i+1}} - t_{\alpha_i} = n_i\pi/\omega_d$ is very large, as in far-future response prediction. By contrast, continuous solutions are generated by the Chebychev polynomial approximation, and therefore this would easily allow construction of modal displacement vectors with a common time base.

8.2. DISPLACEMENT RESPONSE HISTORY PREDICTION WITH INTERMITTENT EXCITATION

Figure 14(a) shows a section of intermittent random forcing obtained by generating a section of discrete white noise which has then been amplitude-modulated by three (Gaussian) shape functions with random mean and variance. By randomly positioning these excitation functions at positive locations, the total section shows obvious quiet periods: i.e., where there is no activity. A very high bandwidth has been chosen with fixed $\Delta\tau = 9{\cdot}765 \times 10^{-6}$ s, giving a Nyquist frequency of 51 kHz. This forcing has been applied to transient displacement prediction for an oscillator with a natural frequency of 100 Hz and 0·1% critical damping. Figure 14(b) shows 12 cycles of predicted displacement via the scheme described in section 8.1, compared with a Laplace/IFFT solution of section 2. The state-transition interval is 0·01 s and the $O(\Delta\tau^4\Delta f''')$ phased displacement predictions are shown as "*" and "·" symbols respectively. The Chebychev polynomial solution method is applied using all these displacements as boundary conditions with 0·2% convergence criterion in equation (102), and restricting the maximum degree of polynomial to degree 20. The error between the detailed Chebychev solution and the Laplace/IFFT method is also shown in Figure 14(b). Figure 14(c) shows a similar comparison between the Laplace/IFFT solution and the $O(\Delta\tau^2\Delta f')$ recursive state-transition algorithm (examined in section 4). This shows no visible error between these two methods but the $O(\Delta\tau^2\Delta f')$ algorithm is orders of magnitude slower taking more than 100 times the CPU time of the Laplace/IFFT solution. By contrast, these 12 cycle predictions via the two-stage scheme described in section 8.1 take a very similar CPU time for the Laplace/IFFT solution, but the Laplace solution, as shown in Figure 14(b), is more accurate. Figure 15(a) shows a section of intermittent excitation and, as a backdrop, the Chebychev polynomial degree needed to obtain each of the 20 solution cycles shown in Figure 15(b). In this example, the Chebychev polynomial degree is restricted to a maximum of 30. Figure 15(b) again includes a comparison with the Laplace/IFFT solution, where the error is also identified. The $O(\Delta\tau^4\Delta f''')$ phased displacements are again shown by the "*" and "·" symbols. In this

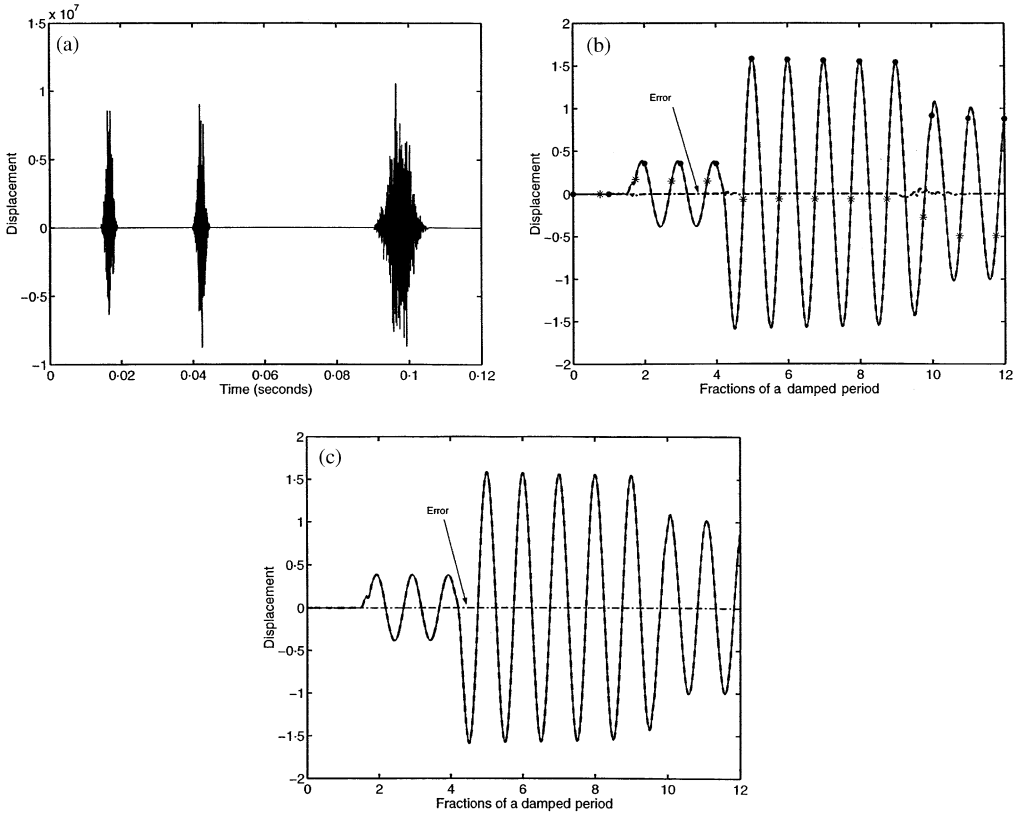

Figure 14. Displacement prediction and errors. (a) Intermittent random white-noise excitation; (b) new two-stage method ("·" and "*" plus Chebychev polynomial solution) compared with Laplace/IFFT; (c) single-step transition method compared with Laplace/IFFT solution showing error.

case, the CPU time of the two-stage method is almost twice as fast as the Laplace/IFFT solution.

8.3. FAR-FUTURE DISPLACEMENT RESPONSE HISTORY PREDICTION

One of the main advantages of the two-stage scheme is that optimum $O(\Delta\tau^4\Delta f''')$ phased displacements, maintain very high accuracy in amplitude and phase over many cycles even though the local (detailed) solution obtained via the adaptive Chebychev polynomial approximation will not be equally accurate. This means that the scheme can be used to do long simulations very efficiently when interest is focused only on the final sections of response. In other words, if 10 000 cycles were to be simulated, but only the details of the last 10 cycles were of interest, then the two-stage scheme is a very efficient way to do it. Figure 16(a) shows a section of intermittent random forcing and Figure 16(b) shows a comparison between the two-stage scheme and a Laplace/IFFT solution. Figure 16(a) again also shows the Chebychev polynomial degree as a backdrop. The relative CPU time performance of the proposed scheme compared with the Laplace/IFFT solution has been examined for an increasing number of transient cycles. Figure 17 shows the CPU time ratio as a function of the total number of cycles, for the case where only the last 10 cycles are of

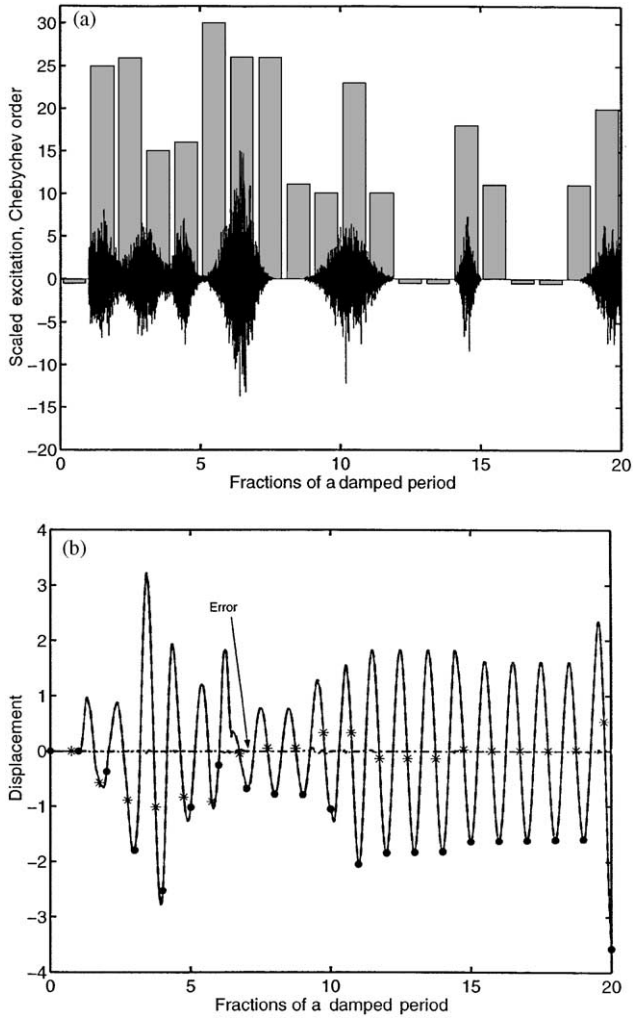

Figure 15. Far-future displacement prediction with intermittent random excitation via new two-stage method. (a) Chebychev order adapted per section (last 10 cycles), showing scaled excitation sample; (b) response comparison with Laplace/IFFT solution.

interest. The CPU ratio up to a maximum of 300 transient cycles is shown, again for 51 kHz sampling rate, being an appropriate PC memory limitation imposed on a single-section Laplace/IFFT solution. The monotonically decreasing behaviour of these relative CPU times suggests that the two-stage scheme has very marked benefits for far-future response prediction. In particular, when the number of cycles approaches 10^4, the CPU time ratio, would be less than 10^{-4}, which in this role, makes the scheme far superior to the Laplace/IFFT solution.

8.4. NON-STATIONARY DENSITY ESTIMATION

The power of the fast integration scheme described in section 8.1 is now demonstrated in two test examples in which oscillator response histories are generated for non-stationary density estimation in a direct Monte Carlo approach. Since the development of the fast

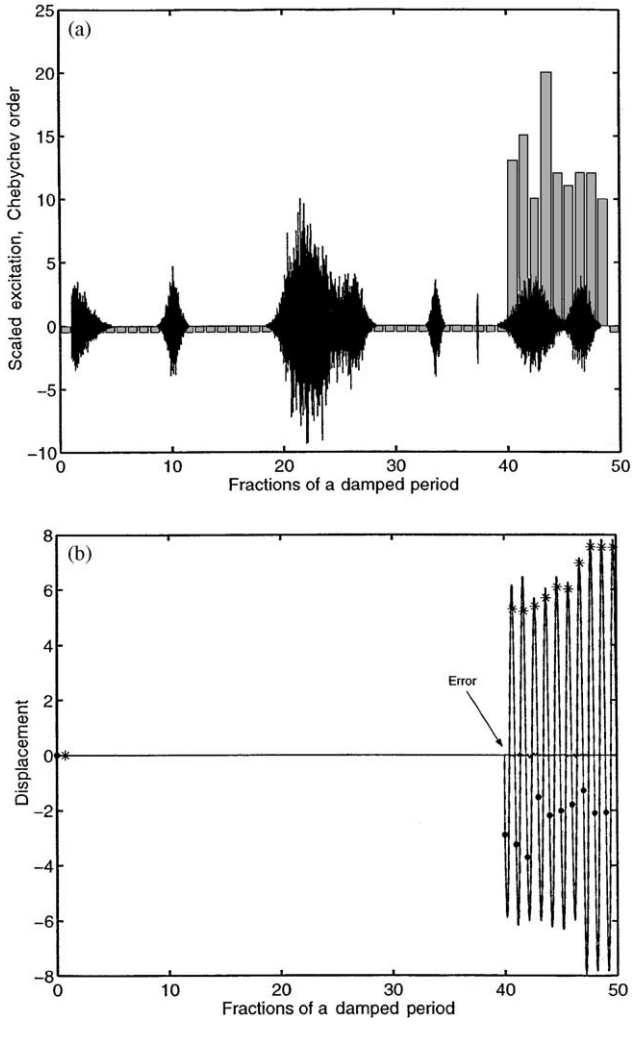

Figure 16. Selected displacement response to intermittent random excitation via new two-stage method. (a) Chebychev order adapted per selected section, showing scaled excitation sample; (b) response for selected sections compared with Laplace/IFFT solution.

integration scheme involved no specific restrictions being placed on the distribution of the discrete excitation process, similar accuracy and efficiency should be obtainable for general forcing. The scheme is now applied to non-stationary probability density estimation for which exact prediction by using wholly theoretical methods is not generally possible, namely for the non-stationary response prediction for an oscillator with ultra-light damping, driven from the rest by ultra-broad-band stationary non-normal excitation. In the first application, attention is focused on obtaining the non-stationary displacement density function. The ensemble of response histories needed for this, can be obtained (at small discrete time steps) by using the three-steps of the scheme, but in general, with no great speed advantage over the Laplace/IFFT method. Significant improvements in efficiency can be obtained, as shown in sections 8.2 and 8.3, if response histories involve excitation quiet periods or if attention is focused on "far-future" displacement prediction. For displacement density estimation however, there is in fact another way the time-domain scheme can be

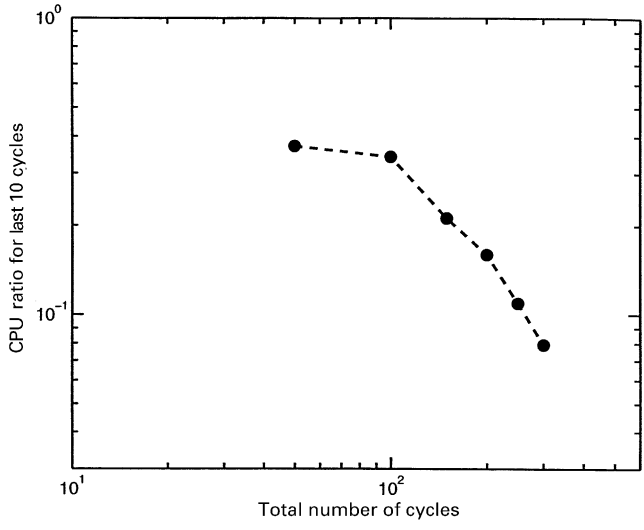

Figure 17. CPU ratio in far-future response prediction. New two-stage method versus Laplace/IFFT solution for detailed displacement prediction of last 10 cycles from total number of cycles.

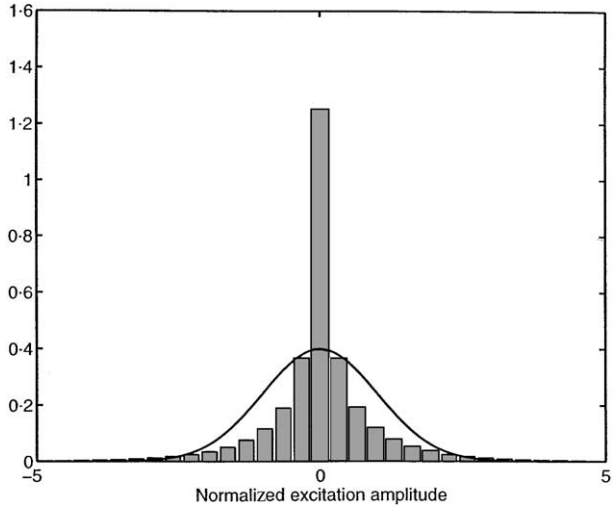

Figure 18. Histogram obtained from non-normal excitation history compared to normal density function with the same mean and variance.

used with even further significant improvement in efficiency. This is achieved by restricting the estimations of the non-stationary density to particular discrete times. To be specific, if the time separation can be chosen precisely as the oscillator damped natural period, then only Step 1 of the scheme in section 8.1 need be used. But this superfast form of the scheme can only be applied to displacement density estimation. In the second application, attention is focused on obtaining the non-stationary peak probability or local maxima density function at times varying from just a short time after oscillator motion commences, to a relatively very long duration. The peak probability density function is important for example in fatigue damage assessment for narrow-band random responses—more details

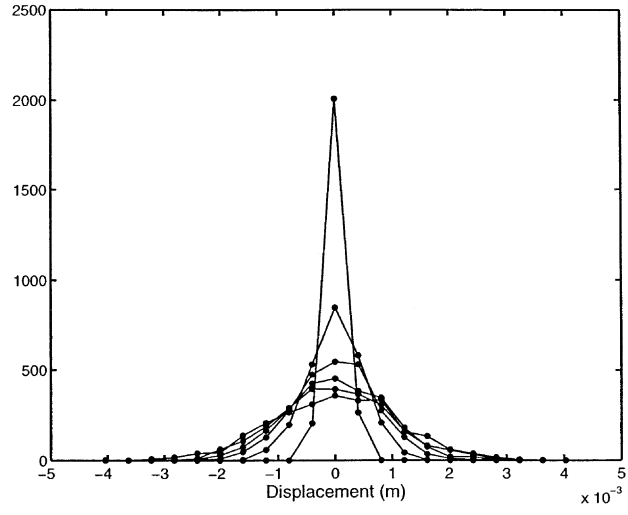

Figure 19. Non-stationary displacement density estimates at six discrete times from start, shown at 1, 10, 20, 30, 40 and 50 damped natural periods (sample size = 1000). —, superfast method (Step 1 of new scheme); ●, estimates via Laplace/IFFT method.

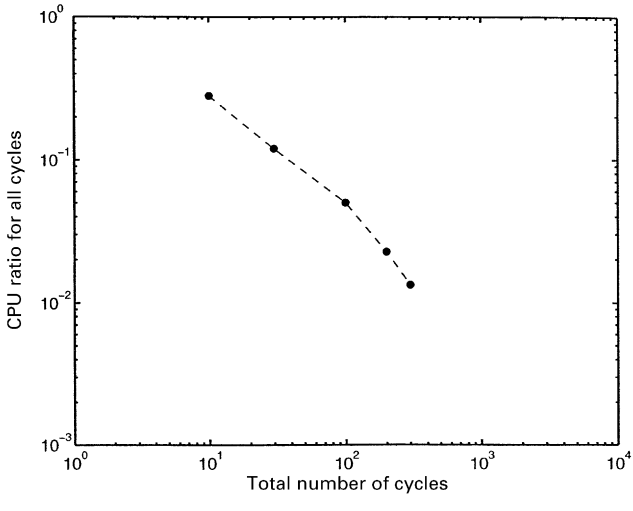

Figure 20. CPU time ratio: superfast method (Step 1 of new scheme) versus Laplace/IFFT method.

on how non-stationary peak densities can be estimated are given shortly. Here, all three steps of the scheme in section 8.1 are needed to obtain selectively detailed response information, but the particular efficiency of the scheme in the role of "far-future" prediction is fully realized. In both examples, comparisons are made wherever appropriate or wherever possible with density estimates obtained by using histories with the Laplace/FFT solution.

Before describing the results of these two applications, a comment is appropriate about the sources of non-normal excitation on space structures, and in particular about the form of excitation chosen to demonstrate the power of the fast algorithm. Examples of the various forcing mechanisms responsible for random excitation on space structures are given

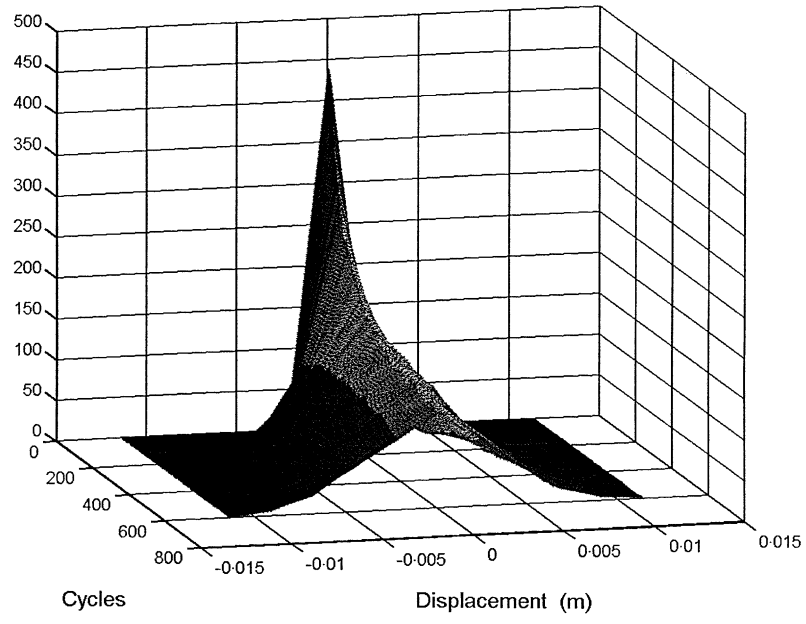

Figure 21. Non-stationary displacement density function, estimated from oscillator responses obtained via superfast method (Step 1 of new scheme) at discrete times 0, 1, 2, … , 600 damped periods. Sample size = 1000.

in section 1. In general, modal excitation functions are obtained through calculation or from measured data. Calculation is in general an enormous task when temporal and spatial dependence is fully taken into account. If experimental data are used, then it can be misleading to assume a modal excitation function is normal on the basis of limited experimental evidence. For example, in the case of fluid turbulence, to construct random excitation histories, a detailed understanding of the structure of turbulence is generally required. Although measurement of flow velocities at a single location may be approximately Gaussian, experimental evidence confirms that joint probability density functions of turbulent flow velocities can be strongly non-Gaussian. The implications of this in the case of turbulence (and elsewhere), are that detailed modal excitation forces are likely to be strongly non-normal. It is also unlikely that a simple functional transformation can be found to generate excitation histories from normal processes which simultaneously meets the required target distribution and spectral properties—to achieve this, quite sophisticated algorithms are needed [30]. For testing purposes, however, the use of simple functional transformations are indeed useful for generating non-normal excitation.

Here, for both the following examples, non-normal excitation histories are generated by using the transformation $Q|Q|$ applied to a stationary Gaussian white noise process Q, without concern for the change this produces to the spectral content. To be precise, the band-limited white noise source Q is sampled at time steps $\Delta\tau = 9{\cdot}7656 \times 10^{-6}$ s, and the magnitude of the forcing standard deviation is chosen as $|\sigma_Q| = 16$.

Starting with the first application, a sample of the excitation pdf is shown in Figure 18 compared with a normal process with the same mean and variance to demonstrate its departure from normality. The bandwidth of the excitation is 51 200 Hz. Figure 19 shows non-stationary displacement density estimates obtained by using the superfast time-domain algorithm (Step 1 of the fast scheme) compared with estimates based on the Laplace/IFFT method at six discrete times from start, namely at 1, 10, 20, 30, 40 and 50 damped natural

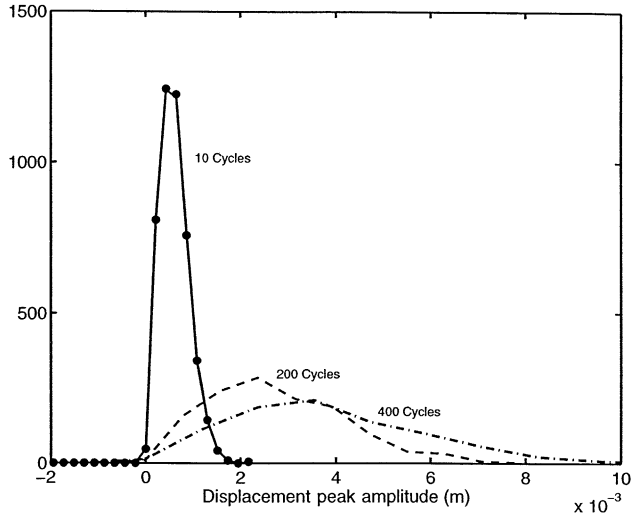

Figure 22. Non-stationary peak probability density estimates (local maxima pdf) via new scheme (Steps 1–3) showing time from start as a parameter at 10, 200, and 400 oscillator-damped natural periods. ●, estimate at 10 cycles via Laplace/IFFT method. (Sample size = 1000 for both methods).

periods. In both cases 1000 samples were included in the ensemble. Here it is evident that the accuracy of the pdf obtained by using the superfast scheme is indistinguishable from the Laplace/IFFT method. Figure 20 shows the relative computing times of the two methods, showing that the efficiency of the superfast scheme is considerable. Indeed, it is clear that the superfast scheme can be used to generate the non-stationary displacement density for long periods of time for which the Laplace/IFFT method would be totally impractical. To demonstrate this, the superfast scheme has been further applied to obtain non-stationary displacement density up to 600 cycles, again using 1000 samples. Figure 21 shows the resulting estimate of the non-stationary displacement pdf in the form of a surface plot. It is clear from Figure 20 that the Laplace/IFFT method would have required around 800 times as long to generate the same amount of data for this relatively long duration of non-stationary density function. But when the super-fast scheme is used, only discrete values of the response are obtained, which are not useful if derivative information is needed, such as, for obtaining peak probabilities.

In the second example, the full scheme of section 8.1, is used on the same 100 Hz oscillator with the same damping and non-normal excitation to obtain non-stationary peak probability density function estimates at specific times, namely after a short time, and after extremely longer periods. A collection of data needed to estimate the peak density function of a non-stationary process actually requires local maxima samples at identical times. In practice, it is impossible to simulate such data, since sample maxima will occur at different times. For stationary processes, sample peaks can be collected and used to construct the density by assuming the local maxima process to be ergodic. For non-stationary maxima, it is necessary to use a short time window in which very little change occurs in the statistical properties of the peaks. The probability density function can then be estimated from data captured within that window to give an estimate of the density function at the centre of the window. Here, the time window chosen corresponds precisely to two single periods. The three steps of the fast scheme (section 8.1) have been applied at three discrete times corresponding to 10, 200, and 400 cycles respectively. A comparison with the Laplace/IFFT

method for the 10-cycle application is shown in Figure 22. This confirms that the new scheme generates probability density estimates which are again indistinguishable from those obtained with Laplace/IFFT method. But in the other two cases (200 and 400 cycles), the Laplace/IFFT method is far too slow and therefore not practical (in this case, the CPU ratio ranges somewhere between Figure 17 and Figure 20).

9. CONCLUSIONS

A new time-domain method has been developed for computing displacement histories of single linear oscillators with arbitrarily light damping and ultra-high-bandwidth discrete forcing. This can be of particular use for obtaining long-duration amplitude and phase associated with undamped response of s.d.o.f. and normal-mode systems with high-bandwidth non-normal random excitation. The paper shows the following.

- In general, non-stationary history prediction requires very high bandwidth, much higher than that needed for stationary histories. Zero-padding is needed for sub-sectioned solutions via fast Laplace/IFFT solution, which cannot readily exploit intermittent excitation or prediction in the far-future.
- The local truncation error associated with simple trapezoidal-based recursive integration does not converge for single transitions involving discrete-time white noise excitation. However, in multiple transitions, this error is shown not to be propagated, allowing accurate (but very slow) recursive time-domain integration.
- Detailed error analysis using the Euler–Maclaurin summation formula, reveals that for integration over a finite transition interval using band-limited white noise excitation, the best interval is any integer multiple of the damped natural period, where the velocity equation is not needed, and where the $O(\Delta\tau^2\Delta f')$ truncation error can be trivially evaluated. This culminates in a computationally very simple optimal $O(\Delta\tau^4\Delta f''')$ scheme, which is shown to be more accurate than any other fixed-step integration scheme (of higher, lower, or equal order).
- This optimal $O(\Delta\tau^4\Delta f''')$ scheme can be used on its own with single oscillators to obtain "super-fast" displacement predictions at selected discrete times, giving massive speed advantages over all the alternatives examined.
- By combining this optimum $O(\Delta\tau^4\Delta f''')$ scheme with an adaptive Chebychev polynomial solution, continuous displacement histories can be obtained for selected cycles in a newly proposed 'two-stage" method.
- This combined two-stage method is in general faster than simple trapezoidal-based recursive integration by at least a factor of 100.
- For general applications, the proposed two-stage scheme is marginally faster than fast Laplace/IFFT solution, with further improvements being realized for intermittent excitation. But for non-stationary density estimation involving history prediction in the far-future (such as for peak probability density estimation), the speed advantage over the fast Laplace can be enormous, varying in practice by a factor between 10 and 10 000.

The overall conclusion then for non-stationary density estimation using Monte Carlo simulation of oscillator motion with very light damping and ultra-high-bandwidth discrete-time non-normal forcing, is that the simplicity of the fast Laplace/IFFT method makes it best for short-term history prediction. But for special applications involving history prediction into the very far-future, the proposed fast time-domain method is vastly more efficient and is thus recommended.

REFERENCES

1. G. PIERSOL 1996 *Shock and Vibration* **3**, 211–221. Procedures to compute maximum structural responses from predictions or measurements at selected points.
2. R. S. LANGLEY and N. S. BARDELL 1998 *The Aeronautical Journal* **102**, 287–297. A review of current analysis capabilities applicable to the high frequency vibration prediction of aerospace structures.
3. J. E. BISHOP and V. K. KINRA 1993 *Journal of Reinforced Plastics and Composites* **12**, 210–226. Thermoelastic damping of a laminated beam in flexure and extension.
4. S. L. FOLKMAN, E. A. ROWSELL and G. D. FERNEY 1995 *Journal of Guidance Control and Dynamics* **18**, 1398–1403. Influence of pinned joints on damping and dynamic behavior of a truss.
5. A. J. BRONOWICKI, N. S. ABHYANKAR and S. F. GRIFFIN 1999 *Smart Materials & Structures* **8**, 740–752. Active vibration control of large optical space structures.
6. M. T. LANDAHL and E. MOLLO-CHRISTENSEN 1992 *Turbulance and Random Processes in Fluid Mechanics*. Cambridge: Cambridge University Press.
7. M. BRASSARD, R-H CHEN and L. CHEW 1996 *Journal of Sound and Vibration* **197**, 255–261. An experimental study of under-expanded square jet noise.
8. M. J. CROCKER 1996 in *Handbook of Fluid Dynamics and Fluid Machinery*, Vol. III (J. A. Schetz and A. E. Fuhs, editors). New York: Wiley.
9. M. BOLTEZAR, M. MESARIC and A. KUHELJ 1998 *Journal of Sound and Vibration* **216**, 697–711. The influence of uneven blade spacing on the SPL and noise spectra radiated from radial fans.
10. L. J. BEMENT and H. A. MULTHAUP 1999 *American Institute of Aeronautics and Astronautics Journal* **37**, 357–363. Determining functional reliability of pyrotechnic mechanical devices.
11. J. P. CONTE and B. F. PENG 1997 *Journal of Engineering Mechanics-American Society of Civil Engineers* **123**, 15–24. Fully nonstationary analytical earthquake ground-motion model.
12. S. F. MASRI, A. W. SMYTH and M. I. TRAINA 1998 *Journal of Applied Mechanics-Transactions of The American Society of Mechanical Engineers* **65**, 398–409. Probabilistic representation and transmission of nonstationary processes in multi-degree-of-freedom systems.
13. Y. BEN-HAIM, G. CHEN and T. T. SOONG 1996 *Journal of Engineering Mechanics-American Society of Civil Engineers* **122**, 325–333. Maximum structural response using convex models.
14. J. H. LIN, W. P. SHEN and F. W. WILLIAMS 1995 *Structural Engineering and Mechanics* **3**, 215–228. A high precision direct integration scheme for non-stationary random seismic responses of non-classically damped structures.
15. J. P. CONTE and B. F. PENG 1996 *Probabilistic Engineering Mechanics* **11**, 37–50. An explicit closed form solution for linear systems subjected to nonstationary random excitation.
16. J. H. LIN, W. P. SHEN and F. W. WILLIAMS 1997 *Engineering Structures* **19**, 586–593. Accurate high-speed computation of non-stationary random structural response.
17. B. F. PENG and J. P. CONTE 1998 *Journal of Engineering Mechanics American Society of Civil Engineers* **124**, 684–694. Closed-form solutions for the response of linear systems to fully nonstationary earthquake excitation.
18. G. MICHAELOV, S. SARKANI and L. D. LUTES 1996 *Structural Safety* **18**, 11–31. Fractile levels for non-stationary extreme response of linear structures.
19. G. MICHAELOV, S. SARKANI and L. D. LUTES 1999 *Structural Safety* **21**, 245–267. Spectral characteristics of nonstationary random processes—response of a simple oscillator.
20. B. BASU and V. K. GUPTA 2000 *Engineering Structures* **22**, 1714–1722. Stochastic seismic response of single-degree-of-freedom systems through wavelets.
21. B. F. SPENCER JR. and L. A. BERGMAN 1993 *Non-linear Dynamics* **4**, 357–372. On the numerical solution of the Fokker–Planck equation for non-linear stochastic dynamics.
22. D. C. K. CHEN and L. D. LUTES 1994 *Journal of Engineering Mechanics-American Society of Civil Engineers* **120**, 814–834. 1st-passage time of secondary system mounted on yielding structure.
23. A. KAREEM, C. C. HSIEH and M. A. TOGNARELLI 1998 *Journal of Engineering Mechanics* **124**, 668–683. Frequency domain analysis of offshore platform in non-Gaussian seas.
24. M. DI PAULA and G. FALSONE 1994 *Probabilistic Engineering Mechanics* **9**, 265–272. Stochastic Dynamics of MDOF structural systems under non-normal filtered inputs.
25. M. D. PANDEY and S. T. ARIARATNAM 1996 *Journal of Engineering Mechanics-American Society of Civil Engineers* **122**, 507–511. Crossing rate analysis of non-Gaussian response of linear systems.
26. G. MUSCOLINO 1995 *Probabilistic Engineering Mechanics* **10**, 35–44. Linear-systems excited by polynomial forms of non-Gaussian filtered processes.
27. M. DI PAOLA and I. ELISHAKOFF 1996 *Chaos Solitons & Fractals* **7**, 961–971. Non-stationary response of linear systems under stochastic Gaussian and non-Gaussian excitation: a brief overview of recent results.

28. M. Di Paola 1997 *Journal of Applied Mechanics-Transactions of the American Society of Mechanical Engineers* **64**, 712–717. Linear systems excited by polynomials of filtered Poisson pulses.
29. G. Muscolino and G. Ricciardi 1999 *Computer Methods in Applied Mechanics and Engineering* **168**, 121–133. Probability density function of MDOF structural systems under non-normal delta-correlated inputs.
30. M. Di Paula and G. Falsone 1998 *Meccanica* **33**, 279–290. Higher order alongwind response statistics of linear SDOF structures including the quadratic term of the fluctuating wind velocity.
31. K. R. Gurley and A. Kareem 1999 *Proceedings of the Fourth International Conference on Stochastic Structural Dynamics, Notre Dame, Balkema*, 31–36. A multi-variate non-Gaussian simulation algorithm.
32. D. E. Newland 1989 *Mechanical Vibrations Analysis and Computation*. New York: Longman Scientific.
33. D. E. Beskos and G. V. Narayann 1983 *Computer Methods in Applied Mechanics and Engineering* **37**, 289–307. Dynamic response of frameworks by numerical Laplace transform.
34. T. Kant, C. P. Arora and J. H. Varaiya 1992 *Composite Structures* **22**, 109–120. Finite-element transient analysis of composite and sandwich plates based on a refined theory and a mode superposition method.
35. C. T. Sun and J. M. Bai 1995 *International Journal of Mechanical Sciences* **37**, 441–455. Vibration of multi-degree-of-freedom systems with nonproportional viscous damping.
36. H. C. Tsai 1998 *Computers and Structures* **66**, 675–683. Modal superposition method for dynamic analysis of structures excited by prescribed support displacements.
37. W. H. Press, B. P. Flannery, S. A. Teukolsky and W. T. Vetterling 1989 *Numerical Recipes —the Art of Scientific Computing*. Cambridge: Cambridge University Press.
38. R. W. Clough and J. Penzien 1993 *Dynamics of Structures*, 89–97. New York: McGraw-Hill, second edition.
39. J. H. Lin, W. P. Shen and F. W. Williams 1995 *Computers and Structures* **56**, 113–120. A high-precision direct integration scheme for structures subjected to transient dynamic loading.
40. J. L. Beck and M. J. Dowling 1988 *Earthquake Engineering and Structural Dynamics* **16**, 245–253. Quick algorithms for computing either displacement, velocity, or acceleration of an oscillator.
41. J. F. Dunne and M. Ghanbari 1997 *Journal of Sound and Vibration* **206**, 697–724. Extreme-value prediction for non-linear stochastic oscillators via numerical solutions of the stationary FPK equation.
42. P. E. Kloeden and E. Platen 1995 *Numerical Solution of Stochastic Differential Equations* (Part V, Strong and weak Taylor approximations, pages 339–506). Berlin: Springer Verlag.

APPENDIX A: LIST OF SYMBOL DEFINITIONS

A, B	system matrices (2×2), in state-space model
A_1, B_1, A_2, B_2	square matrices of dimension $n \times n$ needed for Chebychev polynomial solution
B_n	Bernoulli numbers in Euler–Maclaurin summation formula (EMSF)
$[a, b]$	arbitrary time interval
C_m	complex Fourier coefficients
[C]	damping matrix
c_k	Chebychev polynomial coefficients of a function
c'_k	Chebychev polynomial coefficients of the first derivative of a function
c''_k	Chebychev polynomial coefficients of the second derivative of a function
$\underline{c}$	vector of Chebychev polynomial coefficients
e	total truncation error in trapezoidal integration
e_1	first truncation error term in trapezoidal integration (first error term in the EMSF)
$e_{1_{r.m.s.}}$	r.m.s. value of first truncation error term in trapezoidal integration
e_{upper}	upper bound on truncation error term in trapezoidal integration
$e_{1_{upper}}$	upper bound on displacement truncation error using trapezoidal integration
$e_{2_{upper}}$	upper bound on velocity truncation error term using trapezoidal integration
$e_{\Delta\tau^2}$, $e_{\Delta\tau^4}$, $e_{\Delta\tau^6}$ (r.m.s.)	error terms in the EMSF for specific transitions equal to a damped oscillator period
e_{crit}	error convergence criterion for adaptive Chebychev polynomial solution
f_i	discrete frequency in Hz

f_{max} maximum frequency in Hz
$f(\tau)$ function of time (to be integrated using dummy variable)
f_N Nth discrete value of a function
f'_N Nth discrete value of the derivative a function
$G_1(t, \tau)$ displacement convolution integrand
$G_2(t, \tau)$ velocity convolution integrand
$h(t)$ impulse response function
$\mathrm{H}(\mathrm{j}\omega)$ complex frequency response function
H square matrix needed for Chebychev polynomial solution
I integral sum
I_S integral sum via Simpson's rule
$\mathrm{I}_{r.m.s.}$ r.m.s. value of integral (via trapezoidal rule)
$\mathrm{I}_1, \mathrm{I}_2$ displacement and velocity convolution integrals
$\mathrm{I}_{\Delta\tau}$ integral via Euler–Maclaurin summation formula for step size $\Delta\tau$
$\mathrm{I}_{2\Delta\tau}$ integral via Euler–Maclaurin summation formula for step size $2\Delta\tau$
I_{opt} optimum order displacement transition integral
I_6 sixth order displacement transition integral
I_{Q_j} integrals needed to obtain Chebychev polynomial solution
$\underline{\mathrm{I}}_{N-1}$ contribution to integral at the Nth step
j complex number $= \sqrt{-1}$
$[\mathrm{K}]$ stiffness matrix
$[\mathrm{M}]$ mass matrix
$\underline{\mathrm{p}}(t)$ excitation vector
$\underline{\mathrm{q}}_k$, $q(t)$ displacement response at discrete and continuous time
$\bar{q}_k(s)$ Laplace transform of the displacement response
$\underline{q}_\alpha$ vector of displacements at discrete times given by vector $\underline{t}_\alpha$
$\underline{q}_\beta$ vector of displacements at discrete times given by vector $\underline{t}_\beta$
$Q_k(t)$ excitation function
r_e ratio: r.m.s. value of integral truncation error/r.m.s. of the integral
r_{e_1} ratio: r.m.s. value of truncation error (first term in EMSF)/r.m.s. of integral
$r_{\Delta\tau^2}, r_{\Delta\tau^4}, r_{\Delta\tau^6}$ ratio: r.m.s. truncation error (of corresponding order)/r.m.s. of integral using EMSF for specific transitions equal to a damped oscillator period
$S_X(\omega)$ power spectral density function
$S_{X^{(n)}}(\omega)$ power spectral density function for the nth derivative of $X(t)$
t time variable
t_i discrete time
t' time variable within interval $[-1, 1]$ (for Chebychev polynomial solution)
T_{max} duration of time needed for FFT solution
T_{pad} duration of zero padding time needed for FFT solution
$\mathrm{T}_n(t)$ Chebychev polynomials of a function of time t
$\mathrm{T}_{M/2}$ half-period of oscillator
$\underline{u}$ input vector in state-space model
$W_b(t)$ continuous-time band-limited white noise process
W_{b_i} discrete-time samples of band-limited white noise process
$\dot{W}_{b_i}$ discrete-time samples of the derivative of a band-limited white noise process
$\ddot{W}_{b_i}$ discrete-time samples of the second derivative of band-limited white noise process
$\underline{\mathrm{x}}$ state vector
$\underline{\mathrm{x}}_N(t)$ state vector after N transitions
$X(t)$ stationary stochastic process
Z_i uncorrelated random numbers with standard deviation σ_z
$\underline{Z}$ displacement vector in physical co-ordinates
$Z_{Q_k}(\mathrm{j}\omega)$ Fourier-transformed excitation
$Z_{q_k}(\mathrm{j}\omega)$ complex displacement response

Greek letters

$\alpha_{1m}, \alpha_{2m}, \alpha_{3m}$ partial fraction coefficients for Laplace solution
$\underline{\varepsilon}_{N-1}$ truncation error of the Nth step in finite state transitions
$\underline{\varepsilon}_{\mathrm{x}_N}$ propagated truncation error in the state vector

ε_{n1}	relative magnitude of Chebychev polynomial coefficient (type 1)
ε_{n2}	relative magnitude of Chebychev polynomial coefficient (type 2)
$\Delta\tau$	time step size
$\phi_1(t) \ldots \phi_4(t)$	state transition functions
ρ_1, ρ_2	complex conjugate roots of the characteristic equation
σ_z	standard deviation
ω_{nk}	undamped natural frequency
ω_d	oscillator damped natural frequency
ω_m	excitation frequency
ξ_k	damping factor